First-principles theory of short-range order in size-mismatched metal alloys: Cu-Au, Cu-Ag, and Ni-Au

C. Wolverton, V. Ozoliņš, and Alex Zunger

National Renewable Energy Laboratory, Golden, Colorado 80401

(Received 20 October 1997)

We describe a first-principles technique for calculating the short-range order (SRO) in disordered alloys, even in the presence of large anharmonic atomic relaxations. The technique is applied to several alloys possessing large size mismatch: Cu-Au, Cu-Ag, Ni-Au, and Cu-Pd. We find the following: (i) The calculated SRO in Cu-Au alloys peaks at (or near) the $\langle 100 \rangle$ point for all compositions studied, in agreement with diffuse scattering measurements. (ii) A fourfold splitting of the X-point SRO exists in both $Cu_{0.75}Au_{0.25}$ and $Cu_{0.70}Pd_{0.30}$, although qualitative differences in the calculated energetics for these two alloys demonstrate that the splitting in $Cu_{0.70}Pd_{0.30}$ may be accounted for by $T=0$ K energetics while $T \neq 0$ K configurational entropy is necessary to account for the splitting in $Cu_{0.75}Au_{0.25}$. $Cu_{0.75}Au_{0.25}$ shows a significant temperature dependence of the splitting, in agreement with recent *in situ* measurements, while the splitting in $Cu_{0.70}Pd_{0.30}$ is predicted to have a much smaller temperature dependence. (iii) Although no measurements exist, the SRO of Cu-Ag alloys is predicted to be of clustering type with peaks at the $\langle 000 \rangle$ point. Streaking of the SRO peaks in the $\langle 100 \rangle$ and $\langle 1\frac{1}{2}0 \rangle$ directions for Ag- and Cu-rich compositions, respectively, is correlated with the elastically soft directions for these compositions. (iv) Even though Ni-Au phase separates at low temperatures, the calculated SRO pattern in $Ni_{0.4}Au_{0.6}$, like the measured data, shows a peak along the $\langle \zeta 00 \rangle$ direction, away from the typical clustering-type $\langle 000 \rangle$ point. (v) The explicit effect of atomic relaxation on SRO is investigated and it is found that atomic relaxation can produce significant *qualitative* changes in the SRO pattern, changing the pattern from ordering to clustering type, as in the case of Cu-Ag. [S0163-1829(98)03808-9]

I. INTRODUCTION

At temperatures above ordering transitions, intermetallic alloys $A_{1-x}B_x$ often form solid solutions composed of a disordered arrangement of the constituent atoms on (or near) sites of a Bravais lattice. The atoms in these solid solutions are not randomly arranged, but rather possess some degree of short-range order (SRO): The SRO is characterized in real space by the pair-correlation function $\overline{\Pi}_{lmn}$ for the atomic shell (lmn), given by $\hat{S}_i \hat{S}_{i+(lmn)}$ [where $\hat{S}_i = -1(+1)$ if site i is occupied by an $A(B)$ atom] averaged over all symmetry-equivalent pairs of lattice sites. The Warren-Cowley SRO parameter for shell (lmn) is then

$$\alpha_{lmn}(x) = \frac{\langle \overline{\Pi}_{lmn} \rangle - q^2}{1 - q^2}, \tag{1}$$

where the brackets denote a thermal average, and $q = 2x - 1$. For a completely random alloy, the occupation variables $\hat{S}_i$ are uncorrelated, $\langle \hat{S}_i \hat{S}_{i+(lmn)} \rangle = \langle \hat{S}_i \rangle \langle \hat{S}_{i+(lmn)} \rangle = q^2$ for (lmn) (000), and the SRO parameters α_{lmn} are all zero; Hence, the degree of SRO determines the extent to which spatial correlations exist in disordered alloys. In diffraction experiments, these correlations give rise to intensity modulations in the monotonic Laue background between Bragg peaks. Thus, the correlations due to SRO have been experimentally measured in many disordered alloys by extracting the portion of diffuse scattered intensity due to SRO.[1–33] This portion of diffuse scattering due to SRO is proportional to the lattice Fourier transform of $\alpha_{lmn}(x)$,

$$\alpha(x, \mathbf{k}) = \sum_{lmn}^{n_R} \alpha_{lmn}(x) e^{i \mathbf{k} \cdot \mathbf{R}_n}, \tag{2}$$

where n_R is the number of real-space shells used in the transform. The SRO expressed in real space [Eq. (1)] or reciprocal space [Eq. (2)] can be given a simple interpretation: Local "ordering tendencies" (i.e., a preference for unlike atom pairs) is given in real space by $\alpha_{lmn} < 0$ and in reciprocal space by a peak in $\alpha(\mathbf{k})$ "off Γ" $[\alpha(\mathbf{k}) \neq \langle 000 \rangle]$. Local "clustering tendencies" are likewise given by $\alpha_{lmn} > 0$ and a peak in $\alpha(\mathbf{k})$ at $\langle 000 \rangle$. Clearly, the SRO reflects the underlying energetic tendencies of atoms in a solid to prefer like pairs of atoms (A-A or B-B clustering) or unlike pairs (A-B ordering, or anticlustering).

The basic thermodynamic factors affecting SRO can be appreciated as follows: In the canonical ensemble at composition x and temperature T, the thermal average in Eq. (1) is given by

$$\langle \overline{\Pi}_{lmn} \rangle = \sum_\sigma P(\sigma, T) \hat{S}_i \hat{S}_{i+(lmn)}, \tag{3}$$

where the sum extends over all possible configurations and $P(\sigma, T)$ is the probability of each configuration σ:

$$P(\sigma, T) = \frac{1}{Z(x, T)} \exp\left[\frac{-E(\sigma)}{k_B T} \right], \tag{4}$$

where $Z(x, T)$ is the canonical partition function and $E(\sigma)$ is the total energy of configuration σ. This energy is, of course, dependent on the atomic positions $\{\mathbf{R}_i\}$. For instance, one could choose the atomic positions to be "unrelaxed," i.e., on

     <u>57</u>   4332

ideal fcc lattice sites, $\{\mathbf{R}_i\}^0$. We show below that this choice can lead to qualitatively incorrect SRO patterns for the systems studied here. A more correct description of the energy is as a function of ''relaxed'' equilibrium atomic positions $\{\mathbf{R}_i\}^{eq}$, determined by zero-force conditions for all $i = 1, \ldots, N$ atoms

$$\mathbf{F}_i = \frac{\partial E}{\partial \mathbf{R}_i} = 0. \qquad (5)$$

Equations (3) and (4) demonstrate that the SRO is determined by a sampling of all configurations with a probabilistic weighting factor. The problem of predicting the equilibrium SRO pattern for a given alloy at x and T is then to evaluate Eqs. (3) and (4) which requires knowledge of $E(\sigma, \{\mathbf{R}_i\}^{eq})$ for each σ. It is important to notice that we use the *total* relaxed electron+ion energy $E(\sigma, \{R_i\}^{eq})$ of configuration σ. It thus contains (a) the sum of all occupied energy bands, (b) electron-electron Coulomb, exchange, and correlation, and (c) ion-ion terms. In contrast, the popular Fermi surface nesting construct[9] is often used to explain the SRO of Eqs. (1)–(4) by focusing instead on a single total energy term from the sum in (a) alone (the highest occupied band).

Theory and measurements of SRO in alloys formed from metal constituents with large size mismatch are challenging due to the fact that atoms ''relax'' away from their ideal lattice sites and move to energy-lowering positions given by Eq. (5). Even though local atomic relaxation does not alter the *identity* of atoms on given lattice sites (and hence, does not alter $\hat{S}_i$ or σ in general), it does affect the energy $E(\sigma, \{\mathbf{R}_i\}^{eq})$, and hence via Eqs. (3)–(5) will affect the propensity of developing a paticular type of SRO pattern in the alloy. These sometimes large atomic relaxations lead to difficulties in SRO treatments: Theoretically, the size mismatch requires one to treat the energetic effects of large atomic relaxations in all configurations, specifically, both random and partially ordered states [Eq. (3)]. Experimentally, in diffuse scattering measurements, the atomic displacements themselves lead to diffuse scattering, complicating the separation of the portion of diffuse scattering due to SRO. Our calculations include the implicit effect of atomic displacements on $P(\sigma, T)$ and therefore on the SRO contribution to diffuse scattering. However, we are not attempting to calculate the explicit contribution of atomic displacements to the diffuse scattering. A first-principles total-energy method capable of treating not only the chemical effects of SRO but also the energetic effects of atomic relaxations in size-mismatched alloys, the mixed-space cluster expansion, has recently been proposed[34] and shown to accurately describe the atomically relaxed energetics of ordered, random, and partially ordered states.[35] Recent generalizations of the method[36,37] have been developed to incorporate the anharmonic effect of relaxations, and thereby to treat systems with very large size mismatch. Here, we use this method to theoretically determine (and, in some cases, predict) the SRO in several size-mismatched transition- and noble-metal alloys, *including the effects of large atomic relaxations* in Eq. (4). By ''turning off'' various contributions to the energetics (such as that of atomic relaxations), we are also able to explicitly study the effects of atomic relaxations on SRO.

We examine the SRO of *three* fcc-based alloy systems, all with large size mismatch: Cu-Au, Cu-Ag, and Ni-Au. Some results are also shown for Cu-Pd. We choose these systems for the following reasons:

In Cu-Au, the SRO has been thoroughly investigated experimentally, at many compositions and temperatures, particularly for the Cu-rich region of the phase diagram.[5–7,11,13,14,18,31] Cu-Au exhibits compound-forming long-range order (LRO) at low temperatures, with the stable phases being composed mostly of $\langle 100 \rangle$ composition waves. SRO fluctuations are found to be primarily located at or near the ordering-type $\langle 100 \rangle$ points in reciprocal space. Interestingly, although the observed low-temperature LRO of Cu_3Au is *commensurate* (i.e., wave vectors at high-symmetry points), a small fourfold splitting of the $\langle 100 \rangle$ peaks has been observed[8,13,31] for Cu-rich alloys, and recent *in situ* experiments[31] have measured an interesting increase in this splitting with increasing temperature for $Cu_{0.75}Au_{0.25}$. We refer to this as *incommensurate* SRO (i.e., the peak wave vector is off the high-symmetry point). Analogies with model Hamiltonian results, such as those of the 2D axial next-nearest-neighbor Ising (ANNNI) model, have been used[31] to infer the physical mechanism for this ''duality'' between commensurate LRO and incommensurate SRO in Cu_3Au. We examine below the validity of these model Hamiltonian results towards explaining the physics of Cu_3Au.

Cu-Pd alloys also exhibit compound-forming LRO; however, for Cu-rich alloys, the Cu-Pd phase diagram shows a series of long-period superstructures based on the $\langle 100 \rangle$ $L1_2$ compound. Like Cu-rich Cu-Au, the SRO of Cu-rich Cu-Pd alloys also have shown peaks near the $\langle 100 \rangle$ points with a fourfold splitting.[10] The temperature dependence of this splitting has recently been theoretically predicted.[38]

The SRO of Ni-Au has been measured[12] only for an isolated composition and temperature. Surprisingly, even though the LRO of this alloy involves phase separation at low temperatures, the SRO (for temperatures above the miscibility gap) is found to peak along the $\langle \zeta 00 \rangle$ points ($\zeta \sim 0.6$), rather than at $\langle 000 \rangle$, which is the typical wave vector for clustering-type SRO.

The LRO in Cu-Ag alloys is, like Ni-Au, phase separation; however, Cu-Ag remains phase separated up to the melting point. For Cu-Ag, there are no reported measurements of the SRO. We wish to predict it.

II. METHODOLOGY

A direct approach to calculating the equilibrium SRO in solid solutions from Eq. (3) involves computation of $E(\sigma, \{\mathbf{R}_i\}^{eq})$ for all configurations σ. This type of direct approach to study finite-temperature thermodynamic properties, such as SRO, would inevitably run into the problem of the ''configurational explosion:'' Even for a binary alloy system with a modest number of sites N, the number of possible configurations 2^N for which we need to know the energy of Eq. (3) becomes enormous. Additionally, the evaluation of the total energy of even *one* configuration by first-principles means is currently limited to relatively small N by the computational effort of these techniques, which currently scales with N^3. One method used to obtain finite-T

thermodynamics is to perform statistical calculations by means of a Monte Carlo algorithm using an energy functional $E(\sigma,\{\mathbf{R}_i\}^{eq})$ that describes the alloy in question. The Monte Carlo calculations do not explore the entirety of configuration space equally (which is unnecessary and terribly inefficient), but rather efficiently spend most time sampling the energy in regions of configuration space where the energy is close to its thermal average. Still, even with efficient sampling of configuration space, Monte Carlo calculations require that the energy functional be sufficiently computationally inexpensive so that it is easily evaluated for very large unit cells and for many different configurations. Thus, a direct use of the local-density approximation (LDA) to describe $E(\sigma,\{\mathbf{R}_i\})$ in Eq. (4) is impractical. Hence, we wish to use a method whereby one maps LDA alloy energetics onto an energy functional that is sufficiently simple so that Monte Carlo simulations become possible, but also sufficiently accurate to reflect the atomically relaxed LDA energetics of a wide variety of alloy configurations. Such a method, the mixed-space cluster expansion (CE), has been developed[34,39] and applied to several alloy systems.[40,37,36] The CE method relies on a mapping of the alloy energetics onto a generalized Ising-like model: One selects a single, underlying parent lattice (in the case of this paper, fcc) and defines a configuration σ by specifying the occupations of each of the N lattice sites by an A atom or a B atom. For each configuration, one assigns the spin-occupation variables, $\hat{S}_i = \pm 1$ to each of the N sites. Within the Ising-like description of the mixed-space CE, the positional degrees of freedom are integrated out, leaving an energy functional of spin variables only $\hat{S}_i$ which reproduces the energies of *atomically relaxed configurations*, with atomic positions $\{\mathbf{R}_i\}^{eq}$ *at their equilibrium zero-force values* satisfying Eq. (5). The details of construction of this energy functional within the LDA are discussed elsewhere,[34,36] and thus we give here only the salient points.

A. Mixed-space cluster expansion

The expression used for the formation energy (the energy with respect the the compositional average of the alloy constituents) of any configuration σ in the mixed-space CE is

$$\Delta H(\sigma) = \sum_{\mathbf{k}} J(\mathbf{k})|S(\mathbf{k},\sigma)|^2 + \sum_f D_f J_f \overline{\Pi}_f(\sigma)$$

$$+ \frac{1}{4x(1-x)}\sum_{\mathbf{k}} \Delta E_{CS}^{eq}(\hat{k},x)|S(\mathbf{k},\sigma)|^2, \quad (6)$$

where the J's are the interaction energies ("effective cluster interactions"), f is a symmetry-distinct figure comprised of several lattice sites (pairs, triplets, etc.), D_f is the number of figures per lattice site, J_f is the Ising-like interaction for the figure f, and the "lattice-averaged product" $\overline{\Pi}_f$ is defined as a product of the variables $\hat{S}_i$, over all sites of the figure f with the overbar denoting an average over all symmetry equivalent figures of lattice sites. In contrast to some previous approaches, we do not define the energy [left-hand side of Eq. (6)] via parametrized J's. Rather, our approach is based on the fact that we know the left-hand side of Eq. (6) quite accurately from first-principles LDA total energies for simple configurations σ, so we define the interaction energies J_f and $J(\mathbf{k})$ from these energies. Thus, we incorporate at the outset a detailed quantum-mechanical picture (LDA) for interactions, and hence for SRO. Also, we note that the *total* energy of Eq. (4) includes eigenvalue (or one-electron), electrostatic, and exchange-correlation terms. Hence, energetic contributions to the one-electron energies (e.g., the Fermi surface) used previously to discuss SRO are only one of a few terms in the total energy.

The mixed-space CE of Eq. (6) is separated into three parts:

(i) The first summation includes *all pair figures* corresponding to pair interactions with arbitrary separation. These pair interactions are conveniently summed using the reciprocal-space concentration-wave formalism. $J(\mathbf{k})$ and $S(\mathbf{k},\sigma)$ are the lattice Fourier transforms of the real-space pair interactions and spin-occupation variables, J_{ij} and $\hat{S}_i$, respectively. (ii) The second summation includes only *nonpair figures*. The real-space summation of Eq. (6) is over f, the symmetry-distinct nonpair figures (points, triplets, etc.). (iii) The third summation involves $\Delta E_{CS}(\hat{k},x)$, the *constituent strain energy*, defined as the energy change when the bulk solids A and B are deformed from their equilibrium cubic lattice constants a_A and a_B to a common lattice constant $a_\perp$ in the direction perpendicular to $\hat{k}$:

$$\Delta E_{CS}(\hat{k},x) = \min_{a_\perp}[(1-x)\Delta E_A^{epi}(\hat{k},a_\perp) + x\Delta E_B^{epi}(\hat{k},a_\perp)], \quad (7)$$

where $\Delta E_A^{epi}(\hat{k},a_\perp)$ is the energy required to deform A biaxially to $a_\perp$. The constituent strain energy corresponds to the $\mathbf{k}\to 0$ limit of $J(\mathbf{k})$ and takes on different values depending on the direction in which this limit is taken. Thus, the constituent strain energy involves a nonanalyticity in $J(\mathbf{k})$ as $\mathbf{k}\to 0$ and hence corresponds to infinite-range real-space elastic interaction terms. Including these long-range terms explicitly (rather than trying to cluster expand them) removes the $\mathbf{k}\to 0$ nonanalyticity of $J(\mathbf{k})$, and thus significantly enhances the convergence of the CE.[34] The calculated constituent strain energies for several principle directions are shown in Fig. 1 for the Cu-Au, Cu-Ag, and Ni-Au fcc alloy systems. A detailed discussion of the calculation and parameterization of constituent strain energies, including anharmonic elastic strain terms, is given in Ref. 41.

B. First-principles alloy energetics

The following *input* is needed to construct the mixed-space CE Hamiltonian: (i) the total energies of a set of fully relaxed ordered fcc-based compounds [required to fit the values of $J(\mathbf{k})$ and J_f], and (ii) the epitaxial energies $\Delta E_A^{epi}(\hat{k},a_\perp)$ of the alloy constituents [required to compute $\Delta E_{CS}^{eq}(\hat{k},x)$ via Eq. (7)]. The *output* is a Hamiltonian [Eq. (6)] that (i) predicts the energy of any configuration (i.e., not only ordered compounds), even 1000-atom cells or much larger, (ii) possesses the accuracy of fully relaxed, full-potential LDA total energies, and (iii) is sufficiently simple to evaluate so that it can be used in Monte Carlo simulations, and thereby extends LDA accuracy to finite temperatures.
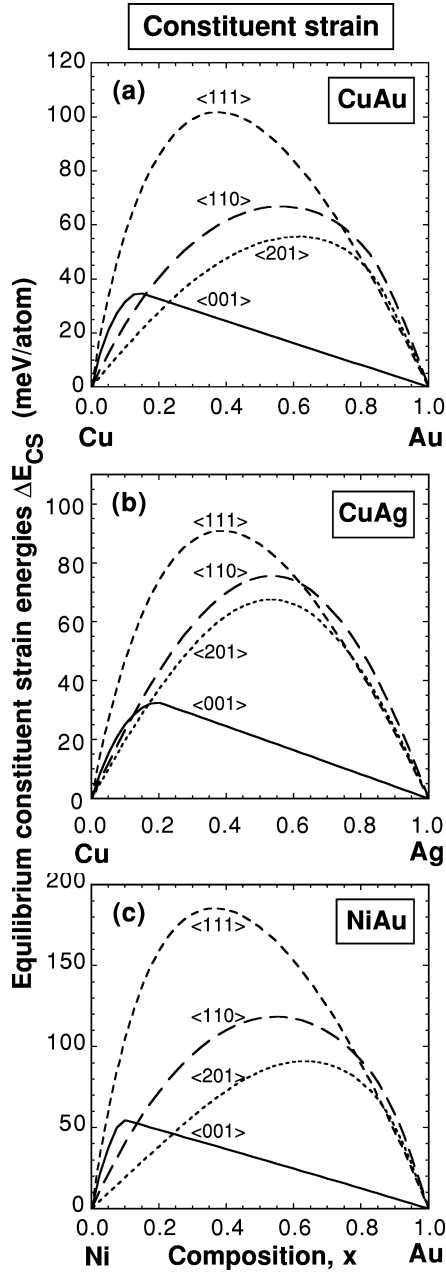
FIG. 1. The calculated constituent strain energies for Cu-Au, Cu-Ag, and Ni-Au along several principle directions.
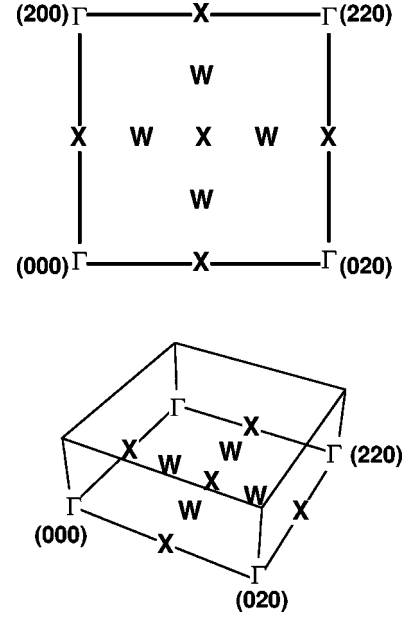

FIG. 2. Schematic plot of $(hk0)$ plane of reciprocal space, with high-symmetry points labeled. The plane is shown from the perspectives used in both the contour and three-dimensional plots in this paper.

Here, we use mixed-space CE Hamiltonians that have been constructed using fully relaxed, full-potential, linearized augmented plane-wave, total energies for the fcc-based Cu-Au, Cu-Ag, and Ni-Au systems. For each alloy, the mixed-space CE has been fit to total energies of $\sim 30-35$ ordered compounds and epitaxial energies for $\sim 5-6$ different orientations (see Ref. 36 for details of the LDA calculations and CE construction for these systems).

C. Monte Carlo details

In order to discern the equilibrium SRO in the alloys of interest here, we have subjected the mixed-space CE of Eq. (6) to Monte Carlo simulations in the canonical (fixed composition) ensemble.[42] We have used fcc unit cells with sizes of $24^3-32^3=13824-32768$ atoms. $\alpha_{lmn}(x)$ are computed

by taking thermal averages of the spin products $\langle \Pi_{lmn} \rangle$ and then using Eq. (1) to obtain the SRO parameters. Using a finite number n_R of these real-space shells in Eq. (2), we obtain the SRO in reciprocal space, $\alpha(x, \mathbf{k})$. Tests have been performed to ascertain the number of Monte Carlo steps required for convergence of the SRO. We have used $\simeq 1000$ Monte Carlo stops (MCS) for taking averages of the SRO; this is preceded by $\sim 100-500$ MCS for equilibration. For SRO in the disordered phase, the Monte Carlo algorithm converges quite quickly; thus, large cell sizes and large number of MCS were only necessary in cases of determining very subtle features of the SRO pattern (e.g., the temperature dependence of the fourfold SRO splitting in Cu-Au or Cu-Pd). We have calculated the SRO using several different random number generators in the Monte Carlo algorithm. Only very subtle features such as SRO splitting were affected in any significant way. We settled on the generator from the ESSL libraries.[43]

For all of the alloys studied here, the $(hk0)$ plane in reciprocal space [which contains the high-symmetry $\Gamma (= \langle 000 \rangle)$, $X (= \langle 100 \rangle)$, and $W (= \langle 1\frac{1}{2}0 \rangle)$ points] contains the SRO peak positions. Therefore, for all SRO plots in reciprocal space, we show only the $(hk0)$ plane. A schematic plot of this plane of reciprocal space is shown in Fig. 2 along with the high-symmetry points.

III. CONSTITUENT STRAIN: RELEVANCE TO SRO

Here we discuss the constituent strain energies [Eq. (7)] for the alloy systems of interest (Cu-Au, Cu-Ag, and Ni-Au) and give some indications of the conditions under which this strain energy is expected to play a major role in determining the SRO. The constituent strain energies for Cu-Au, Cu-Ag, and Ni-Au are shown in Fig. 1 for several principle directions. The strain energies for these three systems look quali-
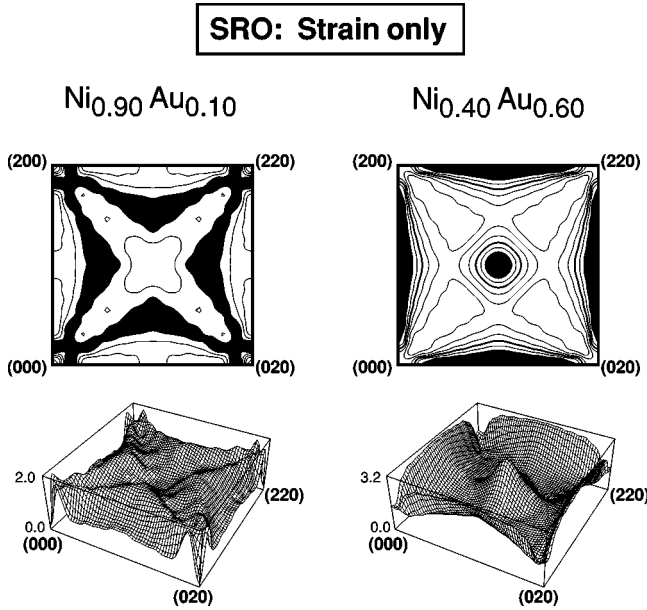
FIG. 3. Monte Carlo–calculated short-range order of $Ni_{0.4}Au_{0.6}$ and $Ni_{0.9}Au_{0.1}$ using constituent strain terms only. Peak intensity (in arbitrary units) is shown by contour shaded black.

tatively similar, with each alloy showing the same crossover of the minimal strain energy with composition: The $\langle 100\rangle$ strain is minimal for alloys where the "large atom" (Au or Ag) is in the majority (e.g., Au-rich Cu-Au, Au-rich Ni-Au, or Ag-rich Cu-Ag). However, for alloys where the "small atom" (Cu or Ni) is in the majority (e.g., Cu-rich Cu-Au, Ni-rich Ni-Au, or Cu-rich Cu-Ag), the $\langle 201\rangle$ direction becomes the elastically softest direction. This crossover of soft strain direction is forbidden in harmonic elasticity theories, and hence is due to anharmonic strain effects.[41]

The energetic effects of constituent strain are expected to be particularly relevant for determining SRO in alloys whose energetics are dominated by strain. In particular, phase-separating alloys are most likely to exhibit "clustered" A-rich or B-rich regions. The strain energy required to maintain coherency between these A-rich and B-rich regions is physically related to the constituent strain energy. Thus, we expect the constituent strain to be most relevant for deciding the SRO tendencies in phase-separating alloys (Cu-Ag and Ni-Au), and less so in ordering alloys (Cu-Au). As we show below, we indeed see manifestations of the crossover of the elastically soft direction on the SRO of Cu-Ag and Ni-Au alloys, but not in Cu-Au.

Equation (6) shows that the alloy Hamiltonian used in the Monte Carlo simulations is composed of three parts: the pair interaction terms, the multibody interaction terms, and the constituent strain terms. We show below calculations of SRO using all three parts of the Hamiltonian. However, given the discussion of the relevance of constituent strain to SRO, it is interesting to see the SRO pattern produced by considering the constituent strain *only*. Thus, in addition to the "full" calculations, which contain pairs, multibodies, and constituent strain in the alloy Hamiltonian, we have also computed the SRO with the CS energy only. These results are shown in Fig. 3, where we have used the $Ni_{0.4}Au_{0.6}$ and $Ni_{0.1}Au_{0.9}$ alloys as examples. From Fig. 1 it is clear that the constituent strain energy is very similar for the three alloy systems, so

we do not expect the "strain-only" results for Ni-Au to be qualitatively different from Cu-Au or Cu-Ag at analogous compositions. (Because the CS energy is nonanalytic in reciprocal space about the origin, many Fourier coefficients are required to converge the SRO of CS alone, thus we use 100 shells of parameters in Fig. 3.) One can see that the SRO with CS only is dominated by almost constant streaks of intensity along the $\Gamma-X$ and $\Gamma-W$ lines, for Au-rich and Ni-rich alloys, respectively, with very little intensity elsewhere. These SRO patterns are understandable when one considers that the soft elastic direction is $\langle 100\rangle$ and $\langle 201\rangle$ for Au-rich and Ni-rich alloys, respectively. Thus, in Au-rich alloys, $\langle 100\rangle$-type fluctuations in the random alloy are energetically favored, and because the constituent strain is dependent only on direction and not on the length of the wavevector, one should expect that all fluctuations along the (100) direction will occur roughly equally, regardless of the length of the wave vector. This expectation is confirmed by the results in Fig. 3. Similarly for Ni-rich alloys, $\langle 201\rangle$-type fluctuations are favored, giving rise to the streaks of intensity along $\Gamma-W$.

IV. SHORT-RANGE ORDER IN $Cu_{1-x}Au_x$

Cu-Au is one of the first alloy systems for which SRO measurements exist.[3] Since then, many other measurements have been carried out for a variety of alloy compositions via both electron diffraction[44–48] and x-ray diffraction.[5–7,11,13,14,18,31] Many of the early investigations have not adequately accounted for displacements. There has also been one previous calculation of the SRO of $Cu_{0.50}Au_{0.50}$ from LDA energetics.[49] The Cu-Au system has historically served as the prototypical Ising-like alloy system for LRO, in that its phase diagram shows ordered compounds[50–53] ($L1_0$ and $L1_2$) that can be stabilized by a simple nearest-neighbor Ising model. In much the same way, Cu-Au has also historically served as the prototypical ordering system in terms of SRO fluctuations: Measurements from Cu-rich to Au-rich compositions have shown peaks in the SRO pattern at (or near) the X point ($\langle 100\rangle$ point). Detailed measurements show a fine structure of the SRO peaks with a small fourfold splitting of the peaks off the X point.[8,9,13,31] The stable long-range ordered compounds in the Cu-Au system ($L1_0$ and $L1_2$) are also composed of $\langle 100\rangle$-type composition waves, and thus for this system there seems to be a (near) coincidence between dominant wave vectors of long- and short-range order. However, as we show below (and pointed out previously[15,54,55]), this coincidence does not exist for all alloys. For example, below we show cases where the configurational entropy ($Cu_{0.75}Au_{0.25}$) and the strain energetics (Ni-Au) shift the free-energy minimum and hence the peak in the high-temperature SRO relative to the low-temperature long-range ordered state. A detailed discussion of the various classes of long- and short-range order in alloys is given in Ref. 55.

A. Effects of composition

Figure 4 shows the calculated SRO patterns in reciprocal space for $Cu_{1-x}Au_x$ over a range of compositions, $x=0.25$, 0.50, and 0.75. The SRO patterns all show large intensities at the $\langle 100\rangle$ point (X point):
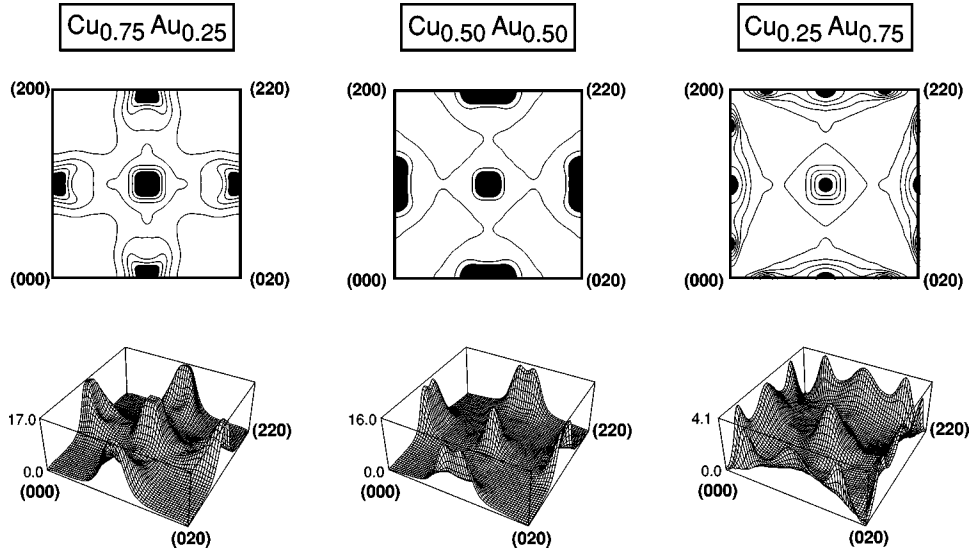
FIG. 4. The calculated SRO patterns in $Cu_{0.75}Au_{0.25}$, $Cu_{0.5}Au_{0.5}$, and $Cu_{0.25}Au_{0.75}$ for $T=550$ K, 670 K, and 800 K, respectively. Peak intensity is shown by contour shaded black. Contours are separated by 4, 5, and 0.7 Laue units, respectively.

(i) $Cu_{0.75}Au_{0.25}$: The LRO of Cu_3Au is of $L1_2$ type, characterized by $\langle 100 \rangle$ composition waves. The SRO of $Cu_{0.75}Au_{0.25}$ shows a very slight fourfold splitting of the calculated SRO peaks off of the X point along the $\langle 1\zeta 0 \rangle$ direction. This fourfold splitting has been measured, and these measurements will be compared with the calculated splitting and will be discussed in detail in Secs. IV B and IV C. The comparison of calculated real-space Warren-Cowley SRO parameters α_{lmn} [Eq. (1)] with those from several experimental measurements for $Cu_{0.75}Au_{0.25}$ are given in Table I, showing good agreement with the measured values (note that of the experimental data cited, Ref. 18 is probably the most modern, at-temperature measurement): Almost all values fall well within the spread between different experimental values. The first- (second-) neighbor parameters are predicted to

be the dominant parameters, having strong ordering (clustering) tendencies, in agreement with all the measured values. After the first and second neighbors, the next largest parameter is calculated to be for the fourth-neighbor shell, with another cluster tendency. Again, this aspect of the calculation agrees with the measured values. [Note that the reciprocal-space SRO pattern of $Cu_{0.75}Au_{0.25}$ is clearly of ordering type, even though two of the three largest real-space SRO parameters (second- and fourth-neighbor) are positive, indicating clustering in these shells. Thus, it it easier to determine the overall clustering/ordering tendency by examining the pattern in reciprocal space, rather than by examining individual α_{lmn} in real space.] The biggest discrepancy between calculated and measured values is in the third-neighbor shell. The calculations give a negative (ordering)

TABLE I. Comparison of calculated Warren-Cowley SRO parameters α_{lmn} with measured values for $Cu_{0.75}Au_{0.25}$ alloys. Values of α_{000} are as measured except in cases denoted by ''1.000'': In these experiments, all SRO parameters have been normalized by the measured value of α_{000}.

Shell	Calculated	Measured					
(lmn)	α_{lmn}			α_{lmn}			
	650 K	703 K [a]	678 K [b]	723 K [b]	678 K [c]	723 K [c]	693 K [d]
0 0 0	1.000	0.935	''1.000''	''1.000''	1.280	1.140	1.107
1 1 0	−0.170	−0.134	−0.152	−0.148	−0.218	−0.195	−0.093
2 0 0	0.257	0.158	0.186	0.172	0.286	0.215	0.141
2 1 1	−0.027	0.007	0.009	0.019	−0.012	0.003	0.035
2 2 0	0.087	0.039	0.095	0.068	0.122	0.077	0.050
3 1 0	−0.032	−0.040	−0.053	−0.049	−0.073	−0.052	−0.099
2 2 2	0.045	0.010	0.025	0.007	0.069	0.028	0.018
3 2 1	−0.004	−0.008	−0.016	−0.008	−0.023	−0.010	−0.006
4 0 0	0.034	0.031	0.048	0.042	0.067	0.036	0.075
3 3 0	−0.022	−0.011	−0.026	−0.022	−0.028	−0.015	−0.019
4 1 1	−0.018	0.009	0.011	0.020	0.004	0.007	0.017

[a]Reference 18. At temperature, displacement corrected.
[b]Reference 3. No size correction.
[c]Reference 7. Quenched.
[d]Reference 11.

TABLE II. Comparison of calculated Warren-Cowley SRO parameters α_{lmn} with measured values for $Cu_{1-x}Au_x$ alloys.

Shell (lmn)	Calculated α_{lmn}			Measured α_{lmn}		
	$Cu_{0.75}Au_{0.25}$ $T=650$ K	$Cu_{0.5}Au_{0.5}$ $T=670$ K	$Cu_{0.25}Au_{0.75}$ $T=800$ K	$Cu_{0.75}Au_{0.25}$ $T=703$ K [a]	$Cu_{0.5}Au_{0.5}$ $T=700$ K [b]	$Cu_{0.25}Au_{0.75}$ $T=573$ K [c]
0 0 0	1.000	1.000	1.000	0.935	1.263	0.992
1 1 0	−0.170	−0.128	−0.032	−0.134	−0.187	−0.071
2 0 0	0.257	0.316	0.147	0.158	0.230	0.103
2 1 1	−0.027	−0.110	−0.045	0.007	−0.013	−0.027
2 2 0	0.087	0.150	0.034	0.039	0.109	0.044
3 1 0	−0.032	0.000	0.003	−0.040	−0.029	−0.023
2 2 2	0.045	0.089	−0.008	0.010	0.030	0.022
3 2 1	−0.004	−0.023	−0.012	−0.008	−0.018	−0.001
4 0 0	0.034	0.097	0.030	0.031	0.037	0.028
3 3 0	−0.022	0.021	0.006	−0.011	−0.006	0.006
4 1 1	−0.018	−0.081	−0.006	0.009	−0.001	−0.005

[a]Reference 18.
[b]Reference 32.
[c]Reference 14.

value of $\alpha_{211}=-0.027$, one measurement[7] gives a slightly weaker ordering value of $\alpha_{211}=-0.012$, but all the other measured values give clustering values $\alpha_{211}>0$. It is interesting to note that the one measurement that gives $\alpha_{211}<0$ was performed for alloys quenched from two different temperatures and found the value of this parameter to be quite sensitive to temperature, with α_{211} getting more negative with decreasing temperature. [The calculations were performed at a temperature ($T=650$ K) 38–73 K lower than the measured values.]

(ii) $Cu_{0.5}Au_{0.5}$: The calculated SRO of $Cu_{0.5}Au_{0.5}$ shows a very small splitting, but at this composition, the calculated splitting is twofold along the $\langle\zeta00\rangle$ direction. A comparison of calculated and measured real-space SRO parameters for various compositions $Cu_{1-x}Au_x$ is given in Table II. For the sake of space, we have only listed one set of measured SRO parameters for each composition (somewhat arbitrarily, the most recent data found for each composition). Comparison of calculated and measured data shows that in almost all cases, the trends of α_{lmn} with composition are accurately reflected in the calculations.

(iii) $Cu_{0.25}Au_{0.75}$: The calculated SRO splitting along $\langle\zeta00\rangle$ increases for Au-rich compositions, and the SRO of $Cu_{0.25}Au_{0.75}$ now shows two distinct peaks: one at $\langle100\rangle$ and one at $\langle\zeta00\rangle$ with $\zeta\sim0.4$. The SRO peak at $\sim\langle0.4,0,0\rangle$ in $Cu_{0.25}Au_{0.75}$ is correlated with the LDA-predicted ground-state structure at this composition:[36] Although experimental evidence for structural determination in $CuAu_3$ seems inconclusive due to difficulties in obtaining equilibrated long-range ordered samples, it is commonly assumed[50–53] that $CuAu_3$ crystallizes in the $L1_2$ structure (characterized by $\langle100\rangle$ composition waves). Yet our total energy, full-potential, all-electron, atomically relaxed LDA calculations indicate[36] that at $CuAu_3$ stoichiometry and $T=0$ K, other ordered compounds have energy lower than the $L1_2$ structure: Specifically, Au-rich Cu-Au superlattices along the $\langle100\rangle$ direction are predicted to be lower in energy than the $L1_2$ $CuAu_3$ structure. These $\langle100\rangle$ superlattices are charac-

terized by composition waves along the $\langle\zeta00\rangle$ direction. An explanation is given in Ref. 36 for the low energy of these $\langle100\rangle$ superlattices in terms of the low constituent strain energy of Au-rich Cu-Au along the $\langle100\rangle$ direction (see Fig. 1). One should note that *unrelaxed* LDA total energies [i.e., with all atoms fixed on ideal fcc sites] will erroneously predict that the $L1_2$ phase is stable at $CuAu_3$ composition, highlighting the importance of atomic relaxation in theories of SRO. Thus, the SRO peak that we find at $\sim\langle0.4,0,0\rangle$ for $Cu_{0.25}Au_{0.75}$ is a fingerprint of the low-energy Au-rich Cu-Au $\langle100\rangle$ superlattices at this composition. To our knowledge, neither the stability of the Cu-Au $\langle100\rangle$ superlattices nor the SRO peak along $\langle\zeta00\rangle$ in Au-rich Cu-Au has been experimentally measured.

B. Existence of SRO peak splitting in $Cu_{0.75}Au_{0.25}$: Comparison with $Cu_{0.70}Pd_{0.30}$

In disordered $Cu_{0.75}Au_{0.25}$, diffuse scattering measurements[8,9,13,31] have shown that the peak intensity due

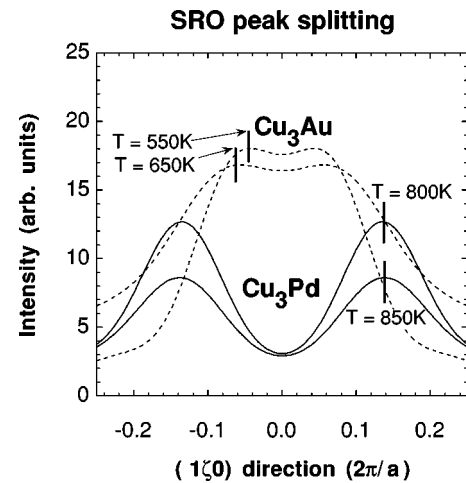FIG. 5. The calculated temperature-dependence of the SRO splitting in $Cu_{0.75}Au_{0.25}$ and $Cu_{0.70}Pd_{0.30}$.
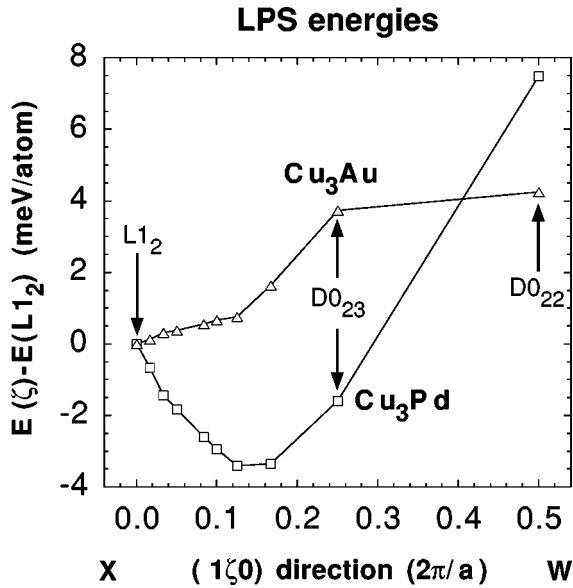
LPS energies

FIG. 6. Structural energies $\Delta E(\zeta=1/2m)=E(\zeta)-E(L1_2)$ of m-period $L1_2$-based long-period superstructures in Cu_3Au and Cu_3Pd as a function of "fundamental" wave vector, $\langle 1\zeta 0\rangle$, where $\zeta=1/2m$. The energies of $L1_2$, $D0_{22}$, and $D0_{23}$ structures, corresponding to $m=\infty$, 1, and 2, are shown by arrows.

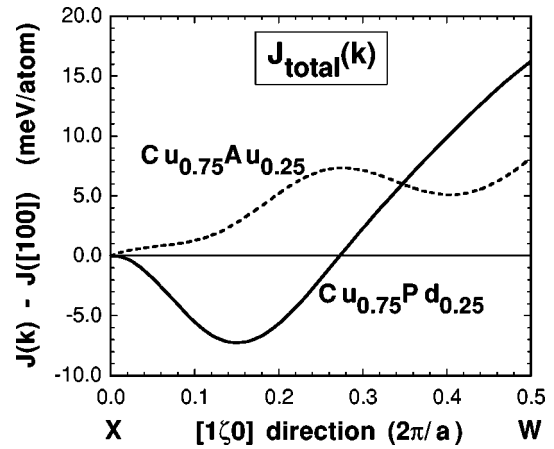FIG. 7. $J_{total}(\mathbf{k})$ (consisting of pair, multibody, and constituent strain terms (Ref. 63) along the $\langle 1\zeta 0\rangle$ line in reciprocal space for Cu_3Au and Cu_3Pd. $\zeta=0(1/2)$ corresponds to the $X(W)$ point, characterized by $L1_2$ $(D0_{22})$-type composition waves.

to SRO is not precisely at the X point, but rather that there is a fourfold splitting of this peak in the $\langle 1\zeta 0\rangle$ direction. Reichert, Moss, and Liang[31] have recently measured the temperature dependence of this splitting *in situ* and have observed, interestingly, an increase in splitting with increasing temperature. Using our theoretical approach, we have thus examined the fine structure of the SRO peaks in $Cu_{0.75}Au_{0.25}$ as a function of temperature in an effort to ascertain the origin of (1) the fourfold splitting itself, and (2) the temperature-dependence of said splitting. Another alloy for which X-point fourfold splitting has been observed[10] is $Cu_{0.70}Pd_{0.30}$. First-principles calculations[56,57,38] have reproduced this peak splitting in $Cu_{0.70}Pd_{0.30}$ at fixed temperature. Additionally, near Cu_3Pd stoichiometry, long-period superstructures are observed at low temperatures, in contrast to the situation for Cu_3Au where $L1_2$ is the low-temperature stoichiometric ground state. This makes Cu_3Pd a potentially interesting contrast to Cu_3Au. Because a mixed-space CE for Cu-Pd has already been constructed using LDA energetics,[57] we use this Hamiltonian to examine the fine structure and temperature dependence of the SRO peaks in $Cu_{0.70}Pd_{0.30}$ so as to provide a comparison with the case of $Cu_{0.75}Au_{0.25}$.[58]

Figure 5 shows the calculated SRO intensity in disordered $Cu_{0.70}Pd_{0.30}$ and $Cu_{0.75}Au_{0.25}$ alloys along the $\langle 1\zeta 0\rangle$ line in reciprocal space. Both $Cu_{0.70}Pd_{0.30}$ and $Cu_{0.75}Au_{0.25}$ alloys show a splitting of the SRO peak off the X point, in agreement with measurements. The splitting is quantified by ζ, the distance (in units of $2\pi/a$) of the SRO peak from the X point. The calculated low-T splitting wave vectors in $Cu_{0.70}Pd_{0.30}$ $\zeta=0.13(2\pi/a)$ and in $Cu_{0.75}Au_{0.25}$ $\zeta=0.05(2\pi/a)$ are in excellent agreement with the measured values of $\zeta=0.13-0.14$ (Refs. 59 and 10) and $\zeta=0.05$,[31] respectively.[60]

We wish to determine the thermodynamic origin of (1) the *existence* of SRO splitting in these alloys and (2) the

temperature dependence of such splitting. First, we examine the origin of the *existence* of the splitting. We find that the qualitative differences in the total energies of $Cu_{0.75}Au_{0.25}$ and $Cu_{0.70}Pd_{0.30}$ lead to the conclusion that the SRO splitting in $Cu_{0.75}Au_{0.25}$ cannot be inferred from $T=0$ K energies alone. However, the splitting in $Cu_{0.70}Pd_{0.30}$ can be inferred from $T=0$ K energies alone: Figure 6 depicts the cluster-expanded $T=0$ K structural energies $\Delta E[\zeta=(1/2m)]=E[(1/2m)]-E(0)$ of $L1_2$ "long-period superstructures" (LPS's). One subset of these LPS's are formed from $L1_2$ $(m=\infty)$ by inserting an antiphase boundary every m cells and have "fundamental" superstructure peaks at $(1\zeta 0)$ where $\zeta=1/2m$. (There are, in general, other "harmonic" wave vectors corresponding to lower amplitude composition waves used to build the LPS. For example, see Refs. 61 or 62.) In Cu_3Pd, a structure with an intermediate ($m_0 \sim 3-4$ or $\zeta \sim 0.17-0.12$) value is predicted to be more stable than $L1_2$ ($\zeta=0$) at $T=0$ K. This implies that there is an *energetic* lowering for fluctuations in the disordered $Cu_{0.70}Pd_{0.30}$ alloy of the $\zeta \sim 0.17-0.12$ type that produce splitting in the SRO peaks. For Cu_3Au LPS, however, we find that $\Delta E(1/2m)>0$ at $T=0$ K for all m and therefore these LPS are not ground-state structures, in qualitative contrast with Cu_3Pd. This means that *there is no energetic gain for fluctuations that produce SRO splitting in* $Cu_{0.75}Au_{0.25}$. The fact that the splitting exists nonetheless in our calculations (even though there is an energetic penalty for such splitting) clearly demonstrates that the existence of the calculated SRO splitting in Cu_3Au is due to entropic effects. Further, because the only entropic effect we have included in our calculations is configurational, one can conclude that *configurational entropy is necessary to account for the SRO splitting in* $Cu_{0.75}Au_{0.25}$.

Another way to see the distinction between the energetics of $Cu_{0.75}Pd_{0.25}$ and $Cu_{0.75}Au_{0.25}$ is to examine the Fourier transform $J_{total}(\mathbf{k})$ of the Hamiltonian used to generate the SRO patterns in Fig. 5. Figure 7 shows the calculated $J_{total}(\mathbf{k})$ for $Cu_{0.75}Pd_{0.25}$ and $Cu_{0.75}Au_{0.25}$ along the $\langle 1\zeta 0\rangle$ line in reciprocal space. In these figures, we have included all contributions of the mixed-space CE Hamiltonian of Eq. (6):

$$J_{total}(\mathbf{k})=J_{pair}(\mathbf{k})+J_{MB}(\mathbf{k})+J_{CS}(\mathbf{k}), \qquad (8)$$

where the three terms are the pair interactions, the multibody interactions, and the constituent strain.[63] The minimum in $J_{total}(\mathbf{k})$ for $Cu_{0.75}Au_{0.25}$, which demonstrates the lowest *energy* point along this line, does not occur for some intermediate $\zeta \neq 0$, but rather occurs *at the X point*. Thus, as stated before, the internal energy alone for this Hamiltonian will not produce SRO fluctuations with a fourfold splitting (since there is an energetic penalty for $\zeta \neq 0$ fluctuations). Since our $T \neq 0$ Monte Carlo results using the energetics shown in Fig. 7 nonetheless produce a SRO splitting, we conclude that it is the configurational entropy that moves the minimum in free energy towards some $\zeta \neq 0$ position and hence produces a splitting the SRO peaks.

In qualitative contrast to $Cu_{0.75}Au_{0.25}$, $J_{total}(\mathbf{k})$ for $Cu_{0.75}Pd_{0.25}$ shows a minimum for an intermediate wave vector between the X and W points ($\zeta \sim 0.14$). This means that fluctuations with wave vectors $\langle 1\zeta 0 \rangle$ ($\zeta \sim 0.14$) will be energetically favorable, and thus the thermodynamic origin of the SRO splitting in $Cu_{0.75}Pd_{0.25}$ is energetic rather than entropic.

The duality noted in the Introduction between commensurate LRO and incommensurate SRO in Cu_3Au is analogous to what is expected from the 2D ANNNI model[65]: In this model, if the ratio between the second- and first-neighbor pair interactions is $1/4 < J_2/J_1 < 1/2$, then the resulting LRO is commensurate and the SRO is incommensurate.[65] Furthermore, the splitting in the SRO is temperature dependent. In this region of the ANNNI model where the duality exists, the reciprocal-space pair interaction $J(\mathbf{k})$ has a minimum *off* the high-symmetry points. Thus, the competing interactions manifest themselves at high temperature as incommensurate SRO, while at low temperature the LRO is commensurate due to geometric effects of the lattice. The striking analogy between the predictions of this model Hamiltonian and what has been observed in Cu_3Au has been used to suggest[31] that the *mechanism* at work for Cu_3Au is the one underlying the ANNNI model, i.e., the duality is encoded in the special features of $J(\mathbf{k})$ (''competing interactions''). We have used a microscopic electronic structure model to calculate $J(\mathbf{k})$ *for* Cu_3Au *from first-principles* (Fig. 7), *and find that* $J(\mathbf{k})$ *has an extremum at* the high-symmetry point. This shape of our first-principles calculated $J(\mathbf{k})$ does not lead (in the 2D ANNNI model) to the LRO/SRO duality observed experimentally. However, our calculated LRO and SRO do nonetheless exhibit the observed duality. Thus, we are forced to conclude that the duality is brought about by effects ''outside'' the 2D ANNNI model, and as explained above, the (3D) configurational entropy plays the crucial role.

We next compare our results with the previous theoretical studies of SRO splitting in $Cu_{0.75}Pd_{0.25}$ alloys. Gyorffy and Stocks[56] have computed the effective interaction in $\mathbf{k}$ space for $Cu_{1-x}Pd_x$ alloys using a composition fluctuation perturbation of the Korringa-Kohn-Rostoker coherent potential approximation (KKR-CPA). Although this approach (starting from a perturbation of the completely random alloy, using the muffin-tin approximation, and neglecting relaxation and electron-electron terms in the total energy) is quite different from our own (starting from the full-potential total energies of small-unit-cell ordered compounds, and including relaxation), comparison of the KKR-CPA interaction for $Cu_{0.75}Pd_{0.25}$ (Fig. 3 in Ref. 62) with our $J_{total}(\mathbf{k})$ shown in

Fig. 7 shows surprising similarities: The minimum in the KKR-CPA calculated interaction is along the $\langle 1\zeta 0 \rangle$ direction at the point $\zeta \sim 0.13$, very close to our calculated minimum at $\zeta \sim 0.14$. Also, the energetic difference in $J_{total}(\mathbf{k})$ between the $\mathbf{k}=X$ point and $\mathbf{k}=W$ points is similar in the previous (-18 meV/atom) and current (-16 meV/atom) calculations. Using the calculations of Gyorffy and Stocks, Ceder *et al.*[62] calculated the Cu-Pd LPS phase diagram within the Bragg-Williams mean-field approximation. At Cu_3Pd stoichiometry, the LPS corresponding to $m=4$ ($\zeta=0.125$) is predicted to be stable, just as it is in our calculations (see Fig. 6). We also emphasize that our calculations make no explicit use of the popular ''Fermi surface nesting'' constructs[9,56,66,67] (although the Fermi surface information is implicitly included in each of the total energies calculated). Indeed, the central quantity in our approach is the *total* (electron+nuclear) energy, not just the one-electron piece (to which Fermi surface nesting arguments apply).

C. Temperature-dependence of SRO peak splitting in $Cu_{0.75}Au_{0.25}$: Comparison with $Cu_{0.70}Pd_{0.30}$

Now that we have discerned the thermodynamic origin of the *existence* of the SRO splitting, we turn to its *temperature dependence*. In order to ascertain the temperature dependences of these splittings, we have performed the SRO simulations for more than one temperature. Our calculations (Fig. 5) show a very small increase of the splitting with increasing temperature in $Cu_{0.70}Pd_{0.30}$, and a much larger relative increase in Cu_3Au, the latter being in qualitative agreement with the experiments of Reichert, Moss, and Liang.[31]

The thermodynamic origin of this temperature dependence may also be ascertained from Fig. 7. Because the interactions in our Hamiltonian [Eq. (6)] have no explicit temperature dependence (e.g., due to nonconfigurational effects), the internal energy of a fixed configuration Eq. (6) has no explicit temperature dependence. Thus, $J_{total}(\mathbf{k})$ given in Fig. 7 for $T=0$ K governs the energetic portion of the free energy at all temperatures. Therefore, *any temperature dependence of the SRO splitting must be due to configurational entropy*. However, we have shown in Fig. 5 that there is a significant temperature dependence of the peak position in $Cu_{0.75}Au_{0.25}$, but not in $Cu_{0.70}Pd_{0.30}$. This is due to the difference in $J_{total}(\mathbf{k})$: In $Cu_{0.75}Pd_{0.25}$, the minimum in $J_{total}(\mathbf{k})$ is relatively deep, and thus the SRO peak position is ''pinned'' near $\zeta \sim 0.14$ and temperature-induced entropy effects cannot move the minimum from this position. However, for $Cu_{0.75}Au_{0.25}$, the minimum of $J_{total}(\mathbf{k})$ is extremely shallow near the X point ($\zeta=0$), and thus this allows for the possibility of entropic effects shifting the peak position to $\zeta \neq 0$. Thus, the shape of the calculated $J_{total}(\mathbf{k})$ in $Cu_{0.75}Au_{0.25}$ allows the SRO peak to more easily move. However, it still remains to be explained why the entropy should prefer the $\zeta \neq 0$ wave vector, rather than the high-symmetry ($\zeta=0$) X point. Currently, we do not have an explanation for this entropic preference. Similar effects (movement of modulation wave vector away from the high-symmetry point with increasing temperature) have been seen in studies of the axial next-nearest-neighbor Ising model.[61,64,65]

Two points of caution are in order about the energy scale involved in the calculation of these SRO splittings and about
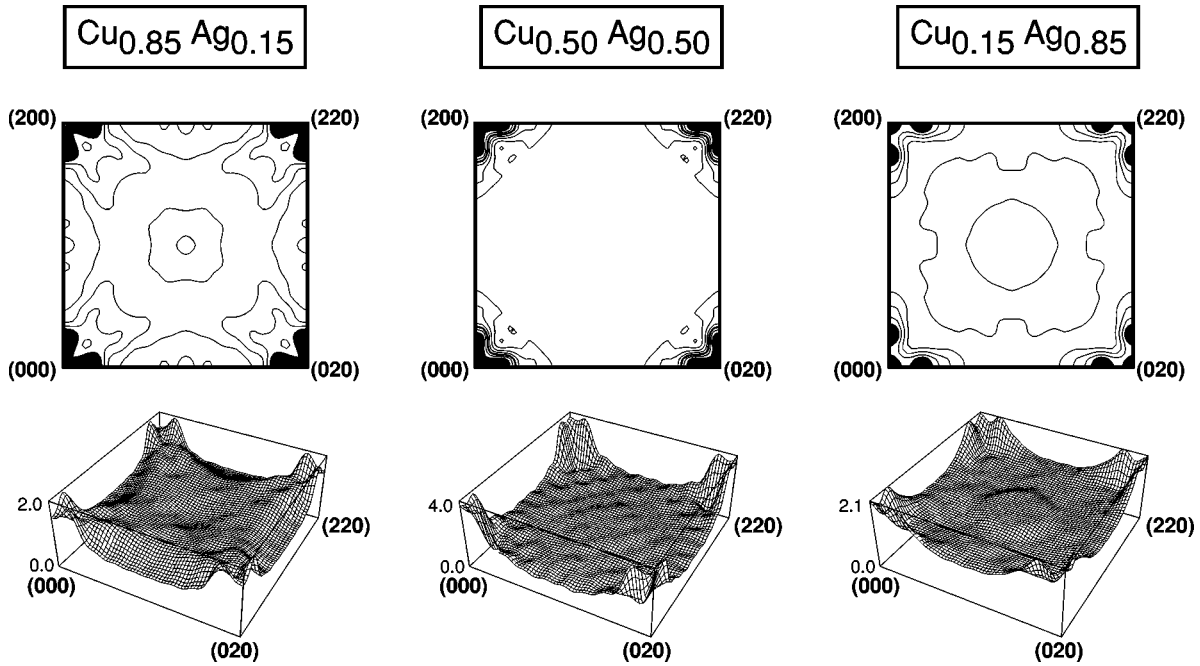
FIG. 8. The calculated SRO patterns in $Cu_{0.85}Ag_{0.15}$, $Cu_{0.50}Ag_{0.50}$, and $Cu_{0.15}Ag_{0.85}$ at temperatures $T=1100$ K, 2000 K, and 1500 K, respectively. Peak intensity is shown by contour shaded black. Contours are separated by 0.2, 0.4, and 0.2 Laue units, respectively.

the prediction of splittings for compositions other than $Cu_{0.75}Au_{0.25}$. One can see from Fig. 6 that the relevant energy scale for this type of problem is $\sim 1-2$ meV/atom, which is beyond the expected accuracy even for ''state-of-the-art'' LDA calculations such as those described here. However, some qualitative effects described here are interesting and valid regardless of slight variations in the energetics involved. For example, we have demonstrated that for the calculated $Cu_{0.75}Au_{0.25}$ Hamiltonian, configurational entropy alone can move the $T=0$ K internal energy minimum (at $\zeta =0$) to a temperature-dependent $\zeta(T) \neq 0$ position at finite

T. The second point of caution is that no statements can be made from this work about the possible splitting of SRO peaks in Cu-Au for alloy compositions other than $Cu_{0.75}Au_{0.25}$. In the approach used here (the mixed-space cluster expansion fitted to LDA total energies), the existence of fourfold X-point splittings are related to the LPS energetics, and thus the SRO peak fine structure is most accurately captured when LPS's are included in the fitting procedure. We have calculated the energies of several of these LPS's for Cu_3Au, but not for CuAu or $CuAu_3$. Although these energetics have not been currently calculated for CuAu or $CuAu_3$,

TABLE III. Predicted Warren-Cowley SRO parameters α_{lmn} for $Cu_{1-x}Ag_x$ alloys.

Shell	Calculated α_{lmn}		
(lmn)	$Cu_{0.85}Ag_{0.15}$ $T=1100$ K	$Cu_{0.50}Ag_{0.50}$ $T=2000$ K	$Cu_{0.15}Ag_{0.85}$ $T=1500$ K
0 0 0	1.000	1.000	1.000
1 1 0	0.018	0.028	0.021
2 0 0	0.033	0.050	0.031
2 1 1	0.008	0.008	0.001
2 2 0	−0.025	0.003	0.002
3 1 0	0.007	0.015	0.005
2 2 2	0.009	0.003	−0.005
3 2 1	0.002	0.004	−0.000
4 0 0	0.016	0.018	0.003
3 3 0	−0.011	0.004	0.002
4 1 1	0.006	0.011	0.004
4 2 0	−0.006	0.005	0.002
3 3 2	−0.000	0.000	−0.002

TABLE IV. Comparison of calculated Warren-Cowley SRO parameters with measured values for $Ni_{0.40}Au_{0.60}$.

Shell (lmn)	Calculated α_{lmn}			Measured α_{lmn}	
	$T=2300$ K	$T=2000$ K	$T=1600$ K	$T=1023$ K (Ref. 12)	Ref. 4[a]
0 0 0	1.0000	1.0000	1.0000	1.047(92)	
1 1 0	−0.0244	−0.0260	−0.0235	0.039(45)	−0.030
2 0 0	0.0806	0.0932	0.1208	0.148(39)	
2 1 1	−0.0119	−0.0138	−0.0134	−0.081(27)	
2 2 0	−0.0096	−0.0089	−0.0021	−0.057(27)	
3 1 0	0.0074	0.0089	0.0164	0.020(24)	
2 2 2	−0.0142	−0.0171	−0.0195	−0.030(26)	
3 2 1	0.0013	0.0016	0.0056	0.039(17)	
4 0 0	0.0181	0.0219	0.0334	−0.018(35)	
3 3 0	−0.0066	−0.0070	−0.0032	−0.084(25)	
4 1 1	0.0055	0.0067	0.0121	−0.022(20)	
4 2 0	−0.0044	−0.0048	−0.0018	0.027(18)	
3 3 2	−0.0061	−0.0071	−0.0062	−0.003(17)	

[a]Early, polycrystalline measurement.

doing so poses no difficulty in principle if one were interested in determining the existence (or absence) of SRO splitting in CuAu or $CuAu_3$.

V. SHORT-RANGE ORDER IN $Cu_{1-x}Ag_x$

$Cu_{1-x}Ag_x$ is quite distinct from $Cu_{1-x}Au_x$ in its low-temperature phase stability. While $Cu_{1-x}Au_x$ forms ordered compounds which disorder and lead to a complete solubility of the solid solution at high temperatures, $Cu_{1-x}Ag_x$ phase separates at all temperatures up to the melting points of both Cu and Ag. There is only limited solubility of Cu in Ag [$\sim 14\%$ at $T=1050$ K (Ref. 51)] and of Ag in Cu [$\sim 5\%$ at $T=1050$ K (Ref. 51)]. Also, different from $Cu_{1-x}Au_x$ where a large number of measurements of SRO exist, to the authors' knowledge, no SRO measurements exist for $Cu_{1-x}Ag_x$ solid solutions.

A. Effects of composition

The calculated reciprocal-space SRO patterns for $Cu_{0.85}Ag_{0.15}$, $Cu_{0.50}Ag_{0.50}$, and $Cu_{0.15}Ag_{0.85}$ are shown in Fig. 8. (The calculated SRO pattern for $Cu_{0.5}Ag_{0.5}$ is "fictitious" in the sense that the measured phase diagram shows phase separation at this composition up to the melting point.) All three patterns show clustering tendencies, indicated by peaks in $\alpha(\mathbf{k})$ at (or near) the Γ point ($\langle 000 \rangle$). However, the peaks are either smeared or slightly split off the origin. The shape of these SRO peaks is consistent with the importance of the constituent strain energy in this phase-separating, large-size-mismatched (12%) Cu-Ag system: In Cu-rich alloys, the clusters of Ag are highly distorted and the strain energy is dominated by the elastic properties of Ag. Figure 1 shows that in Cu-rich Cu-Ag, the lowest strain energy occurs in the elastically soft $[210]=[1\frac{1}{2}0]$ direction. Conversely, for Ag-rich alloys, the strain energy is dominated by Cu. Figure 1 shows that at this limit, the alloy is soft in the [100] direction. The SRO of Cu-rich $Cu_{0.85}Ag_{0.15}$ has a smearing of

the Γ point peak in the $[1\frac{1}{2}0]$ direction, consistent with the Cu-rich constituent strain energy being low in energy in this direction. On the other hand, the SRO of Ag-rich $Cu_{0.15}Ag_{0.85}$ shows a smearing of the peak intensity along the [100] direction, which is elastically soft for Ag-rich compositions. The reason that these arguments connecting constituent strain energy and SRO do not pertain to Cu-Au alloys is explained above in Sec. III: Cu-Au alloys order, rather than cluster, and hence Cu-Au alloys do not sample "clustering-type" configurations.

The predicted real-space SRO parameters for Cu-Ag alloys are given in Table III. Most parameters are small and positive, indicative of a weak clustering tendency. We are not aware of any SRO measurements for this system. Experimental tests of our predictions for Cu-rich or Ag-rich Cu-Ag alloys would be of interest.

VI. SHORT-RANGE ORDER IN $Ni_{1-x}Au_x$

The Ni-Au system, like Cu-Ag, shows phase separation at low temperatures. However, the phase-separating tendency of Ni-Au is weaker than that of Cu-Ag: The top of the miscibility gap occurs at a temperature lower than melting, leaving a completely miscible fcc solid solution at high temperatures. Important early experimental and theoretical work on this alloy includes the work of Moss $et\ al.$,[68,69] Cohen $et\ al.$,[70,12,71] and Cook and de Fontaine.[72] SRO measurements have been performed for Ni-Au,[12] though only for one composition and temperature.

A. SRO of $Ni_{0.40}Au_{0.60}$: Comparison with experiment

The calculated real-space SRO parameters are given in Table IV and compared with those extracted from the diffuse x-ray scattering measurements of Wu and Cohen.[12] The agreement between calculated and measured SRO parameters is reasonable, but not as good as in other alloy systems: The dominant SRO parameter in both theory and experiment
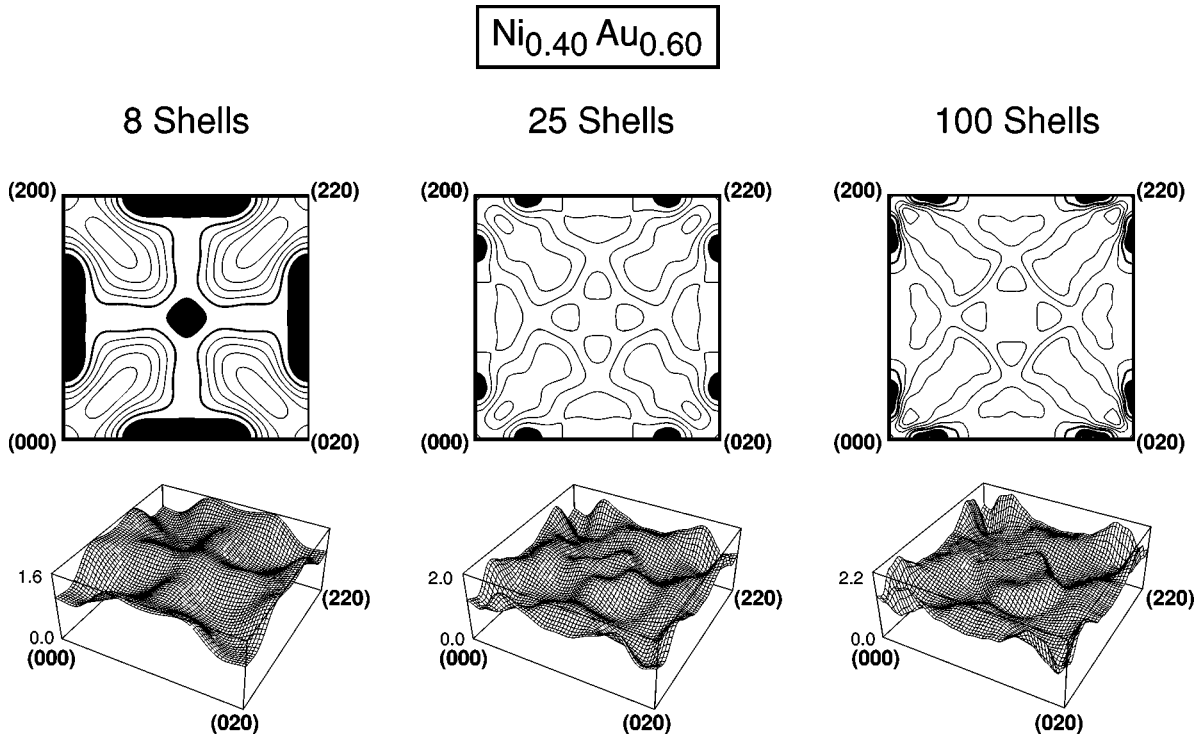
$$Ni_{0.40}Au_{0.60}$$

8 Shells   25 Shells   100 Shells

FIG. 9. Monte Carlo–calculated short-range order of $Ni_{0.4}Au_{0.6}$ in the $(hk0)$ plane using (a) 8, (b) 25, and (c) 100 shells of Warren-Cowley SRO parameters. Peak intensity is shown by contour shaded black. Contours are drawn such that there are ~ 10 contour levels in each plot.

is for the second-neighbor shell, which has a strong clustering-type tendency. Most of the calculated SRO parameters have the same sign as the measured ones, with two notable exceptions: The nearest-neighbor SRO parameter is small and negative in our calculations (indicating a slight ordering tendency in the nearest-neighbor shell), while Wu and Cohen find a small positive (clustering) value. The other discrepancy between calculation and experiment occurs in the (400) shell. It is interesting, however, that the nearest-

neighbor and (400) shells are the only ones for which the experimental error (shown in parentheses in Table IV) is larger than the measured value itself, and thus, the sign of these parameters is in some doubt. We also show in Table IV that earlier x-ray measurements on polycrystalline samples[4] show a nearest-neighbor SRO parameter that is negative.

In measuring the SRO contribution to diffuse intensity, Wu and Cohen reported 25 real-space Fourier shells of SRO parameters. They (1) found a large, positive second-neighbor
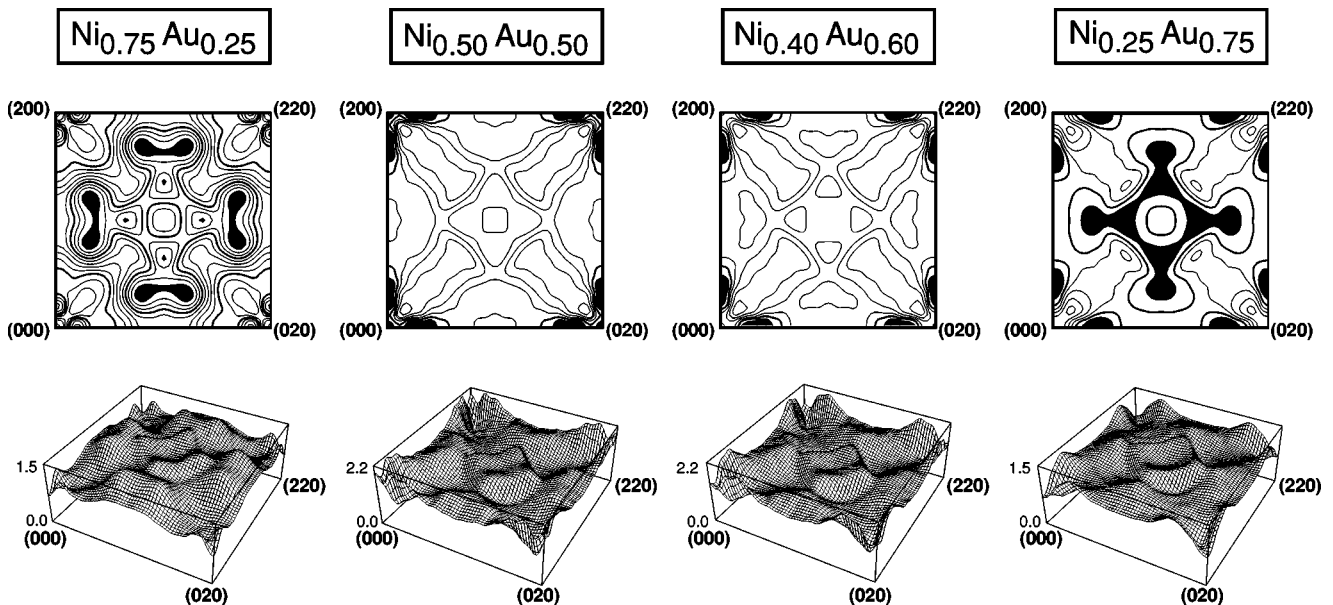
$$Ni_{0.75}Au_{0.25} \qquad Ni_{0.50}Au_{0.50} \qquad Ni_{0.40}Au_{0.60} \qquad Ni_{0.25}Au_{0.75}$$

FIG. 10. The calculated SRO patterns in $Ni_{0.75}Au_{0.25}$, $Ni_{0.50}Au_{0.50}$, $Ni_{0.40}Au_{0.60}$, and $Ni_{0.25}Au_{0.75}$ at $T = 2300$ K. Peak intensity is shown by contour shaded black. Contours are drawn such that there are ~ 10 contour levels in each plot.

Warren-Cowley SRO parameter; and (2) noted, in a simulation based on the measured SRO parameters, clusters of Ni atoms, with the wavelength of these clusters corresponding to the peak of the measured SRO pattern in reciprocal space, $\mathbf{k}_{SRO} \sim (0.6,0,0)$. These facts indicate a short-range *clustering* tendency along the (100) direction. Our calculations agree with these observations. However, there is a semantic problem of how to characterize these facts when considering all of the measured data. We characterize the measured and calculated SRO pattern as *ordering type* since: (1) The total SRO pattern in reciprocal space (including 25 real-space shells) shows peaks *away* from the Γ point, the latter being the typical wave vector for clustering-type tendencies. As we saw in Cu-Au, the gross ordering/clustering tendency is easier to determine by examining the SRO pattern in reciprocal space rather than looking at individual real-space shells. (2) The Warren-Cowley SRO parameters in real space show strong negative (ordering-type) values in many shells *other* than second neighbor, indicating that the clustering tendency in the second shell is competing with an ordering tendency in many other shells.

Several authors have tried to account for the rather surprising result that even though Ni-Au is a phase-separating alloy, the measured peak intensity in reciprocal space due to SRO is of ordering type and occurs at the point $\mathbf{k}_{SRO} \sim (0.6,0,0)$, rather than $\mathbf{k}_{SRO} = (0,0,0)$ which would be expected for a clustering alloy. Lu and Zunger[40] calculated the SRO (using 21 real-space shells) and found peaks at $\sim (0.8,0,0)$ whereas Asta and Foiles[73] used an embedded atom method and found the SRO (using eight real-space shells) to peak at $\sim (0.5,0,0)$. Our calculations for the SRO of $Ni_{0.4}Au_{0.6}$ are given in Fig. 9. We have calculated the SRO at $T=2300$ K, above the miscibility gap temperature for our alloy Hamiltonian.[74] We find that, using 8, 25, and 100 shells, the SRO peaks at $(0.65,0,0)$, $(0.40,0,0)$, and $(0.38,0,0)$ respectively, in reasonable agreement with both the measurements of Wu and Cohen [$\mathbf{k}_{SRO} = (0.6,0,0)$ for 25 shells] and also with previous calculations. If any future SRO measurements on this system are undertaken, one should keep in mind the sensitivity of peak position to the number of real-space shells included in the Fourier transform.

B. Effects of composition

Figure 10 shows the calculated SRO patterns for $Ni_{0.75}Au_{0.25}$, $Ni_{0.50}Au_{0.50}$, $Ni_{0.40}Au_{0.60}$, and $Ni_{0.25}Au_{0.75}$ at $T=2300$ K. Note that since the SRO has only been measured for $Ni_{0.40}Au_{0.60}$, these other calculations represent theoretical predictions. The patterns for $Ni_{0.40}Au_{0.60}$, $Ni_{0.50}Au_{0.50}$, and $Ni_{0.25}Au_{0.75}$ all show peaks between the Γ and X points. However, the SRO pattern for Ni-rich alloys changes in an interesting way: In $Ni_{0.75}Au_{0.25}$, the peaks in the SRO are not along the $\Gamma - X$ line, but rather near the $\Gamma - W$ line ($\langle \zeta \ \zeta/20 \rangle$). As we show below in Sec. VII, unrelaxed energetics are likely to produce ordering-type SRO peaks in this system at "special" or high-symmetry points (Γ, X, W, and L in the case of fcc). However, under certain approximations (pair interactions only, harmonic displacements, and mean-field statistics), Asta and Foiles[73] have proved that a SRO peak that occurs at a high-symmetry point for unrelaxed en-

ergetics, can only be moved off the high-symmetry point towards the origin upon atomic relaxation. This is precisely the effect we see in our calculations: For Au-rich alloys, the low [100] constituent strain energy leads to a large energetic effect of relaxation for [100]-type fluctuations and hence "drags" the SRO peaks off of the X point and towards the origin. In Ni-rich alloys, the [210] constituent strain is lowest in energy and the resulting energetic effect of relaxation drags the SRO peak off the W point towards the origin. In harmonic elasticity theories,[75] only the [100] or [111] strains can be extremal; thus, it is only by including anharmonic effects that one can produce a strain energy minimum in the [210] direction. Thus, the interesting SRO pattern predicted for $Ni_{0.75}Au_{0.25}$ is not only the result of strain effects, but of *anharmonic* strain effects. Any harmonic theory could not hope to capture this effect. It is also interesting to note that the fourfold "ringlike" intensity predicted around the $\langle 110 \rangle$ point (Fig. 10) has been observed in electron diffraction experiments in $Ni_{0.4}Au_{0.6}$ and $Ni_{0.5}Au_{0.5}$.[33]

VII. EFFECT OF ATOMIC RELAXATION OF SHORT-RANGE ORDER

We have demonstrated here a first-principles technique that is capable of predicting the equilibrium SRO for a given alloy system including the effects of atomic relaxation (or atomic displacements). However, we have not investigated the explicit effects of the relaxations themselves on the equilibrium SRO. Unlike experimental measurements of SRO, we can make such an investigation by explicitly "turning off" the effect of atomic relaxation in our calculations, and looking at the resultant effect on the SRO. There have previously been very few theoretical studies examining the effect of atomic relaxation on the SRO,[73] and, to the authors' knowledge, none from a first-principles approach.

In order to examine the effects of relaxation, we must first define precisely what is meant by atomic relaxation and, consequently, what is meant by "unrelaxed" and "relaxed." The formation energy of a given coherent configuration σ may be divided[34] into several parts:

$$\Delta H(\sigma) = \Delta E_{VD}(\sigma) + \delta E_{UR}^{chem}(\sigma) + \delta E^{int}(\sigma) + \delta E^{ext}(\sigma).$$
(9)

The terms on the right-hand side of Eq. (9) are: (i) the volume deformation (VD) energy, defined as the energy required to deform the alloy constituents hydrostatically from their equilibrium lattice constants to that of the alloy structure σ, (ii) the "chemical energy," i.e., the energy difference between an unrelaxed (UR) structure (all atoms at ideal lattice sites) and ΔE_{VD}, sometimes called a "spin-flip" energy, (iii) the energy gained when atomic positions within the unit cell are relaxed, but the unit-cell vectors maintain there ideal angles and lengths, and (iv) the energy gained when the unit-cell vectors are allowed to relax.

In terms of this breakdown of energies, we define "unrelaxed" and "relaxed" energies of coherent, ordered structures in the following way.

Ordered, Unrelaxed: $\Delta E_{VD} + \delta E_{UR}$. The unrelaxed energies included the first two terms of ΔH, but not the later two.

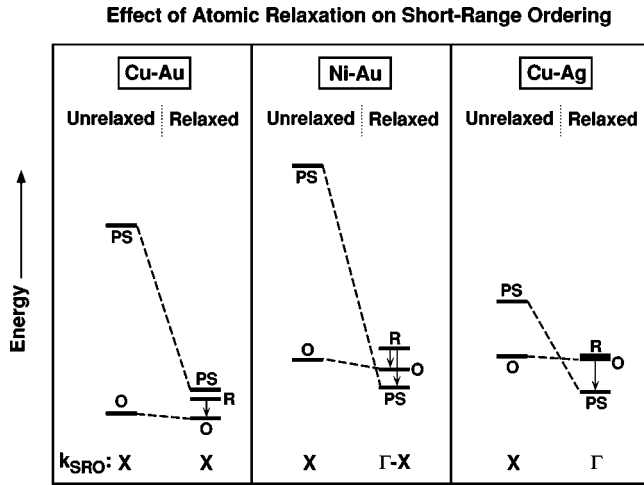**Effect of Atomic Relaxation on Short-Range Ordering**

FIG. 11. Schematic plot of relaxed and unrelaxed energetics of phase-separated and ordered states in Cu-Au, Ni-Au, and Cu-Ag. Although the figure is schematic, the energetics are from first-principles total energies and are drawn to scale. ''PS'' = phase separated; ''O'' = ordered; ''R'' = random. For unrelaxed energetics ''PS'' refers to the energy of deforming the alloy constituents at equiatomic composition hydrostatically to a common volume, $\Delta E_{\text{VD}}(\frac{1}{2})$; ''O'' is the energy of the equiatomic alloy in the $L1_0$ structure, but with all atoms fixed on fcc lattice sites. For relaxed energetics ''PS'' is the equiatomic constituent strain energy in the [100] direction, and ''O'' is the energy of $L1_0$, but allowed to relax to its energy minimum, and ''R'' represents the energy of the atomically relaxed random alloy. Arrows show possible energy-allowed fluctuations of the random alloy towards either ordering (relaxed Cu-Au), phase separation (relaxed Cu-Ag), or both (relaxed Ni-Au). $\mathbf{k}_{\text{SRO}}$ is the SRO peak wave vector for each of these energetic situations.

Thus, this is the formation energy of a structure whose volume is hydrostatically deformed to equilibrium, but all cell-internal and cell-external positions are ideal.

Ordered, Relaxed: $\Delta E_{\text{VD}} + \delta E_{\text{UR}}^{\text{chem}} + \delta E^{\text{int}} + \delta E^{\text{ext}}$. The relaxed energies include all four terms in ΔH. Thus, the difference between unrelaxed and relaxed energies is simply the last two terms, $\delta E^{\text{int}} + \delta E^{\text{ext}}$, the energy gained upon cell-internal and cell-external distortions of the unit cell from their ideal values.

We are interested in SRO in disordered alloys, which is a phenomenon probing *coherent* configurations of atoms, and thus for the interpretations of this section, we must define geometries and energetics that correspond to unrelaxed and relaxed energies of ''coherent ordered'' and ''coherent phase-separated'' states. Because SRO probes the properties of coherent configurations, the energetics of incoherent configurations (such as ''$A+B$'' where A and B are each at their equilibrium lattice constants) are irrelevant to this discussion. We consider a coherent phase-separated configuration to be an infinite-period superlattice, i.e., a A_pB_q stacking of p layers of A and q layers of B along some direction $\hat{G}$ where p and q become infinitely large. (There is of course an interface between A and B in this configuration, but for sufficiently large p and q the energetics of the interface become insignificant relative to the total energy of the superlattice.)

Then, the definitions we used for the unrelaxed and relaxed energies of coherent phase-separated systems are the following.

Phase-Separated, Unrelaxed: ΔE_{VD}. The ''unrelaxed'' geometry of this phase-separated system represents a situation in which both A and B are ideally cubic, but their volumes have been distorted away from equilibrium to the common superlattice volume. This is simply the hydrostatic volume deformation energy defined in Eq. (9).

Phase-Separated, Relaxed: $\Delta E_{\text{CS}} = \Delta E_{\text{VD}} + \delta E^{\text{int}} + \delta E^{\text{ext}}$. Here, atomic positions are fixed in the plane of the interface, but perpendicular to the plane, atoms can move to energy minimizing positions. The energy of this relaxed coherent phase-separated system is precisely the ''constituent strain energy'' defined previously, and shown in Fig. 1.

Therefore, the energy change in going from volume deformation ΔE_{VD} to constituent strain $\Delta E_{\text{CS}}(\hat{G})$ gives an indication of the relaxation of a coherent phase-separated configuration. In terms of the breakdown in Eq. (9), the energies of phase separated configurations do not contain any ''chemical'' energy terms by definition.

With these definitions then, we computed the energetics of unrelaxed and relaxed ordered and phase-separated configurations for the alloys studied here. Figure 11 shows schematically the energetics of a few typical coherent phase-separated (PS) and ordered (O) configurations for Cu-Au, Ni-Au, and Cu-Ag, both in unrelaxed and relaxed geometries at equiatomic composition. Because [100]-type fluctuations seem to be the most important type for the vast majority of the cases we have examined, we show in this figure only [100]-type configurations: $\Delta E_{\text{CS}}([100])$ for the phase-separated configuration, and $L1_0$ for the ordered configuration. For the relaxed energetics, we have also included the energy of the random alloy (R). From this figure, several interesting trends emerge regarding our calculated short-range order patterns, as follows.

Relaxed energetics. When the ordered phase is energetically below phase separation and the random alloy is intermediate, such as CuAu, the energetically favored fluctuations of the random alloy (shown by vertical arrows) are ordering-type (e.g., an X-point peak in SRO). When, phase separation is lower then ordering and the random alloy is nearly degenerate with the ordered phase, such as CuAg, clustering-type fluctuations of the random alloy are favored, and the system exhibits a clustering-type SRO peak (Γ). However, in the case of NiAu, the relaxed phase-separated state is lower than the ordered phase, but the random alloy is higher in energy than either the ordered or coherently phase-separated state. In this case, both ordering-type and clustering-type fluctuations of the random alloy are energetically favored (although clustering-type fluctuations more so). Thus, there is a competition between ordering- and clustering-type fluctutations, and the SRO peak is between the nominally clustering (Γ) and ordering (X) wave vectors.

Unrelaxed energetics. For all three alloys, the energy gain upon relaxation of the phase-separated state is large, but the relaxation of the ordered phase is much less. In all three alloys, unrelaxed energetics demonstrate that the phase-separated state is much higher in energy than the ordered state. (Although we have just plotted one ordered compound in Fig. 11, the qualitative statements about relative energetics

are not effected by our specific choice of ordered compound.) Thus, one would expect that an ordering-type SRO would result for each of the three alloys, constrained to unrelaxed geometries. Calculations using unrelaxed LDA energetics bear out this expectation: Using a technique analogous to that described in Sec. II, we have fit the *unrelaxed* LDA energies of a large number of Cu-Ag compounds to a cluster expansion Hamiltonian. Subsequent Monte Carlo calculation using this Hamiltonian yields a SRO pattern (not shown here) for "unrelaxed Cu-Ag" which is ordering type, with peaks at the X point. Similar X-point ordering-type SRO patterns have been predicted for unrelaxed Cu-Au (Ref. 49) and Ni-Au.[73] Thus, (i) in Cu-Au, the X-point peaks are not qualitatively affected by relaxation, while (ii) in Ni-Au, relaxation moves the SRO peak from the X point toward the origin of reciprocal space to a point along the $\Gamma - X$ line. (iii) In Cu-Ag, relaxation moves the SRO peak from an ordering-type positions (X point) to a clustering type position (near the Γ point), reversing the *qualitative ordering tendencies* of the disordered alloy. These predictions are in accord with the proof of Asta and Foiles,[73] who showed that under certain restrictions, relaxation can only move an ordering-type SRO peak towards the Γ point.

VIII. SUMMARY

In this paper, we have described a first-principles technique for calculating the short-range order (SRO) in disordered alloys, even for alloys with large size mismatch, where harmonic elastic theories are invalid. The technique has been applied to several alloys possessing large lattice mismatch: Cu-Au, Cu-Ag, and Ni-Au. We have demonstrated that the anharmonic strain energetics are most important and can produce qualitatively new effects in the SRO of phase-separating alloys.

Cu-Au alloys. We have found SRO peaks at (or near) the $\langle 100 \rangle$ point for all compositions studied ($x_{Au} = 0.25$, 0.50, and 0.75), in agreement with a wide variety of electron and x-ray diffuse scattering measurements. The calculated real-space Warren-Cowley parameters are also in excellent agreement with those from diffuse scattering measurements. The fine structure of the SRO peak in $Cu_{0.75}Au_{0.25}$ has been examined in detail and compared with the case of $Cu_{0.70}Pd_{0.30}$. A four-fold splitting of the X-point SRO exists in both $Cu_{0.75}Au_{0.25}$ and $Cu_{0.70}Pd_{0.30}$, although qualitative differences in the calculated energetics exist for these two alloys, demonstrating that qualitatively different thermodynamics underlie the peak splitting in these two alloys. By examining both long-period $L1_2$-based superstructures and $J_{total}(\mathbf{k})$ along the $\langle 1\zeta 0 \rangle$ direction of reciprocal space, we were able to see the energetic distinction between $Cu_{0.75}Au_{0.25}$ and $Cu_{0.70}Pd_{0.30}$: We find that for $Cu_{0.70}Pd_{0.30}$ $J_{total}(\mathbf{k})$ exhibits a minimum between the X ($\zeta = 0$) and W ($\zeta = 1/2$) points and, ground-state LPS structures are lower in energy than $L1_2$. However, for $Cu_{0.75}Au_{0.25}$, $J_{total}(\mathbf{k})$ exhibits a minimum at the X point, and the ground-state structure at this composition is $L1_2$. The fact that a SRO peak splitting occurs in $Cu_{0.75}Au_{0.25}$ even though $J_{total}(\mathbf{k})$ is minimal at X demonstrates that at finite temperatures, configurational entropy can shift the SRO peak position from the $T = 0$ LRO value ($\zeta = 0$) to $T > T_c$ values [$\zeta(T) \neq 0$]. Another manifestation of

the qualitatively different energetics in $Cu_{0.75}Au_{0.25}$ and $Cu_{0.70}Pd_{0.30}$ is in the temperature dependence of the SRO splitting. The relatively flat nature of $J_{total}(\mathbf{k})$ near X for $Cu_{0.75}Au_{0.25}$ not only allows the entropy to move the peak position off the X points, but also allows this peak position to be temperature dependent. The calculated temperature dependence of the splitting is in good agreement with recent *in situ* measurements.[31] In contrast, the relatively deep minimum of $J_{total}(\mathbf{k})$ for $Cu_{0.70}Pd_{0.30}$ "pins" the SRO peak position at this energy minimum, and hence, $Cu_{0.70}Pd_{0.30}$ is predicted to have a much smaller temperature dependence.

Cu-Ag alloys. Although no measurements exist, the SRO of Cu-Ag alloys is predicted to be of clustering type, with peaks at the $\langle 000 \rangle$ point. The shape of these calculated SRO peaks is also of interest: Streaking of the SRO peaks was found in the $\langle 100 \rangle$ and $\langle 1\frac{1}{2}0 \rangle$ directions for Ag- and Cu-rich compositions, respectively. These streaks correlate with the elastically soft directions for the constituent strain, a most important contribution to the energetics of this phase-separating, clustering-type alloy. In the absence of atomic relaxation, an X-point peak is predicted.

Ni-Au alloys. Even though Ni-Au phase separates at low temperatures, the calculated SRO pattern in $Ni_{0.4}Au_{0.6}$, like the measured data, shows a peak along the $\langle \zeta 00 \rangle$ direction, away from the typical clustering-type $\langle 000 \rangle$ point. We find that the peak position of the reciprocal-space SRO pattern is quite sensitive to the number of real-space shells used in the Fourier transform. We have also provided predictions of SRO for Ni-Au for $Ni_{0.25}Au_{0.75}$, $Ni_{0.5}Au_{0.5}$, and $Ni_{0.75}Au_{0.25}$. As the Ni composition is increased, we see an interesting movement of the SRO peak position from the $\langle \zeta 00 \rangle$ direction (for Au-rich alloys) to the $\langle \zeta \zeta/2 0 \rangle$ direction for Ni-rich alloys. This shift in SRO peak is correlated with the shift in the elastically soft direction from $\langle 100 \rangle$ to $\langle 210 \rangle$ with increasing Ni content.

Finally, we have explored the explicit effect of atomic relaxation on SRO. Although unrelaxed energetics are likely to produce ordering-type SRO in all the alloy systems studied here, we find that atomic relaxation especially of the coherent phase-separated state can produce significant and even *qualitative* changes in the SRO pattern. For example, in Cu-Ag, the SRO pattern is qualitatively changed from ordering to clustering type upon the inclusion of atomic relaxation. A description of the energetics underlying the coherent phase-separated and ordered states is given and these energies are contrasted with that of the atomically relaxed random alloy. They demonstrate that ordering- (clustering-)type fluctuations are energetically favored in Cu-Au (Cu-Ag), while in Ni-Au both types of fluctuations are allowed, leading to an competition between ordering and clustering, and ultimately to a SRO peak intermediate between the X and Γ points.

[1] M. A. Krivoglaz, *Diffuse Scattering of X-rays and Neutrons by Fluctuations* (Springer, New York, 1996).

[2] L. H. Schwartz and J. B. Cohen, *Diffraction from Materials* (Academic Press, New York, 1977).

[3] J. M. Cowley, J. Appl. Phys. **21**, 24 (1950).

[4] P. A. Flinn, B. L. Averbach, and M. Cohen, Acta Metall. **1**, 664 (1953).

[5] B. W. Roberts, Acta Metall. **2**, 597 (1954).

[6] B. W. Batterman, J. Appl. Phys. **28**, 556 (1957).

[7] S. C. Moss, J. Appl. Phys. **35**, 3547 (1964).

[8] S. C. Moss, in *Local Atomic Arrangements Studied by X-ray Diffraction*, edited by J. B. Cohen and J. E. Hilliard (Gordon and Breach, New York, 1966), pp. 95–122.

[9] S. C. Moss, Phys. Rev. Lett. **22**, 1108 (1969).

[10] K. Ohshima, D. Watanabe, and J. Harada, Acta Crystallogr., Sect. A: Cryst. Phys., Diffr., Theor. Gen. Crystallogr. **32**, 883 (1976).

[11] P. Bardhan and J. B. Cohen, Acta Crystallogr., Sect. A: Cryst. Phys., Diffr., Theor. Gen. Crystallogr. **32**, 597 (1976).

[12] T. B. Wu and J. B. Cohen, Acta Metall. **31**, 1929 (1983).

[13] K.-I. Ohshima, J. Harada, and S. C. Moss, J. Appl. Crystallogr. **19**, 276 (1986).

[14] M. Bessiere, Y. Calvayrac, S. Lefebvre, D. Gratias, and P. Cenedese, J. Phys. (Paris) **47**, 1961 (1986).

[15] F. Solal, R. Caudron, F. Ducastelle, A. Finel, and A. Loiseau, Phys. Rev. Lett. **58**, 2245 (1987).

[16] V. Gerold and J. Kern, Acta Metall. **35**, 393 (1987).

[17] W. Schweika and H.-G. Haubold, Phys. Rev. B **37**, 9240 (1988).

[18] B. D. Butler and J. B. Cohen, J. Appl. Phys. **65**, 2214 (1989).

[19] L. Reinhard, B. Schönfeld, G. Kostorz, and W. Bührer, Phys. Rev. B **41**, 1727 (1990).

[20] B. Schönfeld, J. Traube, and G. Kostorz, Phys. Rev. B **45**, 613 (1992).

[21] K. Koga and K. Ohshima, J. Phys. Condens. Mater. **2**, 5647 (1990).

[22] P. Schwander, B. Schönfeld, and G. Kostorz, Phys. Status Solidi B **172**, 73 (1992).

[23] L. Reinhard, J. L. Robertson, S. C. Moss, G. E. Ice, P. Zschack, and C. J. Sparks, Phys. Rev. B **45**, 2662 (1992).

[24] R. Caudron, M. Sarfati, M. Barrachin, A. Finel, F. Ducastelle, and F. Solal, J. Phys. I **2**, 1145 (1992).

[25] R. Caudron, M. Sarfati, M. Barrachin, A. Finel, F. Ducastelle, and F. Solal, Physica B **180**, 822 (1992).

[26] L. Reinhard and S. C. Moss, Ultramicroscopy **52**, 223 (1993).

[27] M. Barrachin, A. Finel, R. Caudron, A. Pasturel, and A. Francois, Phys. Rev. B **50**, 12 980 (1994).

[28] B. Schönfeld *et al.*, Phys. Status Solidi B **183**, 79 (1994).

[29] V. Pierron-Bohnes, E. Kentzinger, M. C. Cadeville, J. M. Sanchez, R. Caudron, F. Solal, and R. Kozubski, Phys. Rev. B **51**, 5760 (1995).

[30] H. Roelofs, B. Schönfeld, G. Kostorz, W. Bührer, J. L. Robertson, P. Zschack, and G. E. Ice, Scr. Mater. **34**, 1393 (1996).

[31] H. Reichert, S. C. Moss, and K. S. Liang, Phys. Rev. Lett. **77**, 4382 (1996).

[32] E. Metcalf and J. A. Leake, Acta Metall. **23**, 1135 (1975).

[33] J. C. Zhao (private communication).

[34] D. B. Laks, L. G. Ferreira, S. Froyen, and A. Zunger, Phys. Rev. B **46**, 12 587 (1992).

[35] C. Wolverton and A. Zunger, Phys. Rev. Lett. **75**, 3162 (1995).

[36] V. Ozoliņš, C. Wolverton, and A. Zunger, Phys. Rev. B (to be published 15 March 1997).

[37] C. Wolverton and A. Zunger, Comput. Mater. Sci. **8**, 107 (1997).

[38] V. Ozoliņš, C. Wolverton, and A. Zunger, Phys. Rev. Lett. **79**, 955 (1997).

[39] A. Zunger, in *NATO ASI on Statics and Dynamics of Alloy Phase Transformations* (Plenum Press, New York, 1994), p. 361.

[40] Z.-W. Lu and A. Zunger, Phys. Rev. B **50**, 6626 (1994).

[41] V. Ozolņiš, C. Wolverton, and A. Zunger, Phys. Rev. B **57**, 4816 (1998).

[42] K. Binder, *Monte Carlo Methods in Statistical Physics: An Introduction* (Springer-Verlag, New York, 1992); *Applications of the Monte Carlo Method in Statistical Physics*, edited by K. Binder (Springer-Verlag, New York, 1987).

[43] It should be noted that the SRO calculations for Ni-Au here differ from previous calculations using the same CE Hamiltonian (Ref. 37) in the larger cell size used here and in the different random number generator. Negligible differences were found.

[44] H. Raether, Agnew. Phys. **4**, 53 (1952).

[45] K. Sato, D. Watanabe, and S. Ogawa, J. Phys. Soc. Jpn. **17**, 1647 (1962).

[46] M. J. Marcinkowski and L. Zwell, Acta Metall. **11**, 373 (1963).

[47] D. Watanabe and M. J. Fisher, J. Phys. Soc. Jpn. **20**, 2170 (1965).

[48] S. Hashimoto and S. Ogawa, J. Phys. Soc. Jpn. **29**, 710 (1970).

[49] T. Mohri, K. Terakura, S. Takizawa, and J. M. Sanchez, Acta Metall. **39**, 493 (1991); Mohri *et al.* used LDA calculations based on the atomic-sphere approximation, neglected atomic relaxations in their calculations, had interactions of only nearest-neighbor range, and found X-point SRO peaks. (With nearest-neighbor interactions only, it is impossible to reproduce the fine structure of the observed peak splitting about the X point.) As we demonstrate in Sec. VII, the neglect of relaxation in *any* of the systems studied here (Cu-Au, Ni-Au, or Cu-Ag) is likely to produce X-point SRO.

[50] *Phase Diagrams of Binary Copper Alloys*, edited by P. R. Subramanian, D. J. Chakrabarti, and D. E. Laughlin (ASM International, Materials Park, OH, 1994).

[51] R. Hultgren, P. D. Desai, D. T. Hawkins, M. Gleiser, and K. Kelley, *Selected Values of the Thermodynamic Properties of Binary Alloys* (American Society for Metals, Metals Park, OH, 1973).

[52] M. Hansen, *Constitution of Binary Alloys* (Genium, Schenectady, New York, 1985).

[53] T. B. Massalski, *Binary Alloy Phase Diagrams* (ASM International, Materials Park, OH, 1990).

[54] C. Wolverton and A. Zunger, Phys. Rev. B **52**, 8813 (1995).

[55] C. Wolverton and A. Zunger, Phys. Rev. B **51**, 6876 (1995).

[56] B. L. Gyorffy and G. M. Stocks, Phys. Rev. Lett. **50**, 374 (1983).

[57] Z. W. Lu, D. B. Laks, S.-H. Wei, and A. Zunger, Phys. Rev. B **50**, 6642 (1994).

[58] One should note that the Hamiltonian for $Cu_{0.70}Pd_{0.30}$ calculated by Lu *et al.* (Ref. 57) and used in Monte Carlo calculations here utilizes a harmonic form of the constituent strain energy, in contrast to the anharmonic form used here for all other alloy systems.

[59] K. Ohshima and D. Watanabe, Acta Crystallogr., Sect. A: Cryst. Phys., Diffr., Theor. Gen. Crystallogr. **29**, 520 (1973).

[60] By Fourier-transforming the 72 shells of measured SRO parameters given in Ref. 10, one obtains for $Cu_{0.7}Pd_{0.3}$ a SRO pattern with splitting $\zeta = 0.18$ (see e.g., Ref. 40). However, the directly determined splitting observed by diffuse x-ray (Ref. 10) or electron (Ref. 59) diffraction gives a splitting of $\zeta = 0.13 - 0.14$.

[61] G. Ceder, M. De Graef, L. Delaey, J. Kulik, and D. de Fontaine, Phys. Rev. B **39**, 381 (1989).

[62] G. Ceder, D. de Fontaine, H. Dreysse, D. M. Nicolson, G. M. Stocks, and B. L. Gyorffy, Acta Metall. Mater. **38**, 2299 (1990).

[63] Because no long-range multibody interactions were included in the CE, these interactions cannot stabilize any LPS other than $L1_2$ or $D0_{22}$—an interaction with spatial extent of eighth-nearest neighbor is necessary to stabilize even the simplest LPS, $D0_{23}$. Hence, the multibody contribution to $J_{total}(\mathbf{k})$ in Fig. 7 is included simply as a straight line with the endpoints given by the multibody contribution to the energies of $L1_2$ and $D0_{22}$.

[64] D. de Fontaine and J. Kulik, Acta Metall. **33**, 145 (1985).

[65] A. Finel and D. de Fontaine, J. Stat. Phys. **43**, 645 (1986).

[66] S. C. Moss and R. H. Walker, J. Appl. Crystallogr. **8**, 96 (1975).

[67] H. Sato and R. Toth, in *Alloying Behavior and Effects in Concentrated Solid Solutions*, edited by T. B. Massalski (Gordon and Breach, New York, 1965), pp. 295–419.

[68] B. Golding and S. C. Moss, Acta Metall. **15**, 1239 (1967).

[69] B. Golding, S. C. Moss, and B. L. Averbach, Phys. Rev. **158**, 647 (1967).

[70] T. B. Wu, J. B. Cohen, and W. Yelon, Acta Metall. **30**, 2065 (1982).

[71] T. B. Wu and J. B. Cohen, Acta Metall. **32**, 861 (1984).

[72] H. E. Cook and D. de Fontaine, Acta Metall. **17**, 915 (1969).

[73] M. Asta and S. M. Foiles, Phys. Rev. B **53**, 2389 (1996).

[74] The high temperature scale in this system has been shown (Ref. 37) to be due to a neglect of nonconfigurational entropy in our calculations, which has been shown to be large in this system.

[75] D. M. Wood and A. Zunger, Phys. Rev. B **40**, 4062 (1989).